The Role of Myosin-X in a Putative System of Intrafilopodial Transport

Michael Kerber

A dissertation submitted to the faculty of the University of North Carolina at Chapel Hill in partial fulfillment of the requirements for the degree of Doctor of Philosophy in the Department of Cell and Molecular Physiology.

Approved by,

Richard Cheney

Robert Sealock

James Bear

Ken Jacobson

Carol Otey

Abstract

Michael Kerber: The Role of Myosin-X in a Putative System of Intrafilopodial Transport
(Under the direction of Richard Cheney)

My research focuses on the role of the molecular motor, myosin-X (Myo10), in the cellular protrusions called filopodia. Chapter one provides an up-to-date review of Myo10 in a manuscript that is being prepared for submission to the Journal of Cell Science. Chapter two, my main data chapter, was published in Current Biology and describes a novel population of fast-moving Myo10 in filopodia that we discovered using single-molecule imaging techniques. For this paper, I optimized the imaging system used to detect single Myo10 molecules, performed most of the experiments, and made all of the figures. I also helped develop a software program, Kymotracker, that exploits a technique called kymography to track and take measurements of these single molecules in time-lapse videos. In Chapter three, I describe preliminary experiments investigating the role of Myo10 in filopodial adhesions. In Chapter four, I summarize conclusions drawn from my research and discuss important avenues of future research in the field.

Table of Contents

List of Figures

List of Abbreviations

ALK6	activin receptor-like kinase 6
ATP	adenosine tri-phosphate
AU	arbitrary units
BMP6	bone morphogenetic protein 6
CALI	chromophore assisted laser inactivation
CytoD	cytochalasin D
DCC	deleted in colorectal cancer
DIC	differential interference contrast
ECM	extracellular matrix
ER	endoplasmic reticulum
FERM	4.1 ezrin radixin moesin
FRAP	fluorescence recovery after photobleaching
HMM	heavy meromyosin
GFP	green fluorescent protein
LatB	latrunculin B
Myo10	myosin-X

MyTH4	myosin tail homology 4
PBS	phosphate buffered saline
PCR	polymerase chain reaction
PEST	proline, glutamic acid, serine, threonine sequence
PH	pleckstrin homology
ROS	reactive oxygen species
SAH	stable α-helix
TIRF	total internal reflection fluorescence
VASP	vasodilator stimulated phosphoprotein

Chapter 1: Myosin-X: a MyTH4/FERM motor at the filopodial tip

Summary

Myosin-X (Myo10) is a MyTH4-FERM myosin broadly expressed in vertebrate tissues. Myo10 is best known for its role in the formation of filopodia and its striking ability to move within filopodia and accumulate at their tips. Its tail region is implicated in signaling downstream of PI3K, interactions with adhesion-associated proteins, and binding to microtubules. In addition to its central role in filopodia, Myo10 is also required for the proper orientation and length of the mitotic spindle. While biophysical studies of Myo10 have begun to uncover the motor's single-molecule properties, exciting progress has also been made in revealing Myo10's physiological functions. Recent evidence has demonstrated that Myo10 is required for the migration of cells crucial for the development of the nervous system.

Introduction

Myosin motors are an ancient group of proteins capable of moving along actin filaments and binding to cargos via a wide variety of tail domains. Myosin-X (Myo10) contains a unique combination of domains in its tail and is the founding member of its own class of myosins. Together with its closest relatives, the class VII and XV myosins, Myo10 is a member of a larger superclass of myosins defined by the presence of myosin tail homology 4 (MyTH4) and band4.1, Ezrin, Radixin, Moesin (FERM) domains. The

MyTH4-FERM myosins have been implicated in mediating membrane-cytoskeleton interactions in protrusive structures such as stereocilia and filopodia (Oliver et al., 1999). MyTH4-FERM myosins are also evolutionarily ancient, appearing very early in metazoan evolution, although Myo10 is not present in the fly and worm lineages (Odronitz and Kollmar, 2007).

Myo10 was originally discovered in a screen for novel myosins in bullfrog inner ear tissue, but has since been detected in most mammalian tissues (Solc et al., 1994; Yonezawa et al., 2000). It is important to note, however, that its level of expression is orders of magnitude lower than that of the better-known myosin-II. Myo10 is the only myosin to boast multiple pleckstrin homology (PH) domains, which confer the ability to bind directly to the plasma membrane (Berg et al., 2000). Through its unique assortment of PH, MyTH4, and FERM domains and distinctive motor properties, Myo10 appears to play several important roles within the cell (Divito and Cheney, 2008; Sousa and Cheney, 2005). In particular, Myo10 has emerged as a central figure in filopodia.

Filopodia provide a point of contact between a cell and its environment and many cells are thought to rely on these finger-like organelles to probe and interact with their surroundings (Mattila and Lappalainen, 2008). Filopodia are therefore thought to be important for developmental processes that rely on directed cell migration, such as axon guidance and angiogenesis (Eilken and Adams, 2010; Koleske, 2003). Despite clear implications in human health and disease, the mechanisms underlying filopodial formation, maintenance, and function remain largely uncertain. Filopodia consist of a plasma-membrane-encased F-actin bundle, oriented with the actin barbed ends towards the filopodial tip (Wood and Martin, 2002). These tips are the sites of actin

polymerization, which contributes to forces that cause the filopodial actin bundle to continuously slide back towards the cell body, a phenomenon termed "rearward treadmilling" (Medeiros et al., 2006). One likely master regulator of filopodia is Myo10, which localizes to filopodial tips, causes an increase in filopodia number, and moves in a directed manner within filopodia (Berg et al., 2000; Bohil et al., 2006; Kerber et al., 2009). Here we review key progress in understanding Myo10, from its structural and single-molecule properties to its role in organismal development.

Myosin-X structure and biochemical properties

Myo10 contains regions referred to as the head, neck, α-helix, and tail (Figure 1.1). The head of Myo10, like all myosins, consists of a conserved motor domain, able to bind to F-actin and hydrolyze ATP to produce force (Homma et al., 2001). Initial in vitro experiments performed using an "HMM-like" Myo10 construct, which includes only the head, neck, and α-helical domains, indicated that Myo10 moved at ~200-300 nm/s with a processivity somewhere between that of non processive motors like myosin-II and highly processive motors like myosin-Va (Chen et al., 2001). A monomeric head-neck construct exhibited an actin activated ATPase of ~4/s at 25°C and a duty ratio of ~16%, again intermediate between that of nonprocessive and highly processive motors (Kovacs et al., 2005). On the contrary, a shorter head-neck construct used by a different group yielded a much higher actin activated ATPase and duty ratio of 13.5/s and ~60%, respectively (Homma and Ikebe, 2005). These discrepancies illustrate the importance of studying full-length My10 constructs in the cellular environment to establish the motor properties of the native protein.

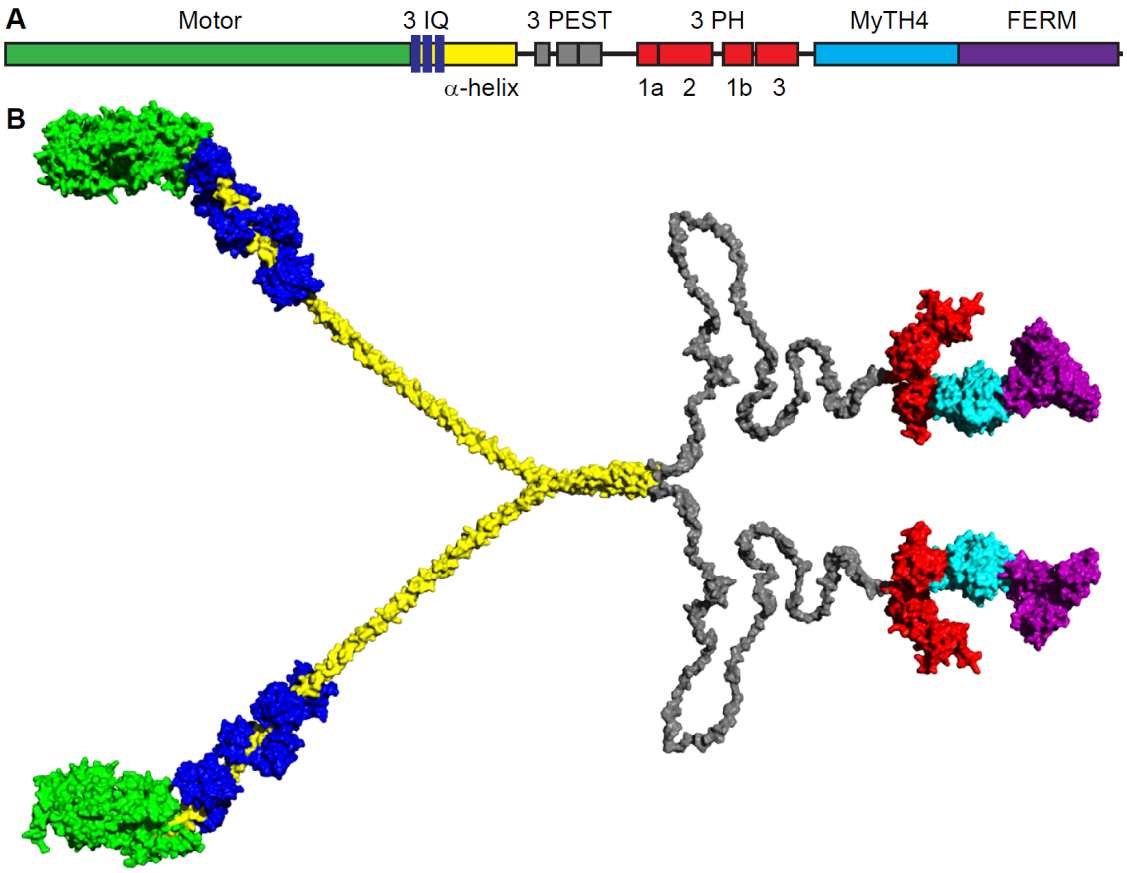

Figure 1.1. Myo10 Structure

(**A**) Domain organization of the Myo10 protein. (**B**) Working model of Myo10's structure, including bound calmodulin light chains (blue), constructed in PyMol by combining domain structures derived from a combination of prediction programs and known domain structures, where possible. Myo10 is depicted here as a dimer with a single-α-helix domain of 90 amino acids and a coiled-coil domain of 40 amino acids, though the exact proportions are unknown. Note that the PEST-domain-containing region (gray) is predicted to be and therefore depicted as a largely unstructured region of roughly 200 amino acids.

Following the motor domain is the Myo10 neck, consisting of three IQ motifs, each capable of binding to calmodulin or calmodulin-like light chains in a calcium-dependent manner (Berg et al., 2000; Homma et al., 2001). Recent studies have shown that calmodulin-like protein actually increases Myo10 expression by interacting specifically with Myo10's IQ3 motif (Bennett et al., 2008; Bennett et al., 2007; Bennett and Strehler, 2008). One explanation for this method of regulation is that during translation, the growing Myo10 peptide somehow interferes with further translation until calmodulin-like protein binds to its neck, changing the conformation of the nascent peptide and allowing translation to proceed (Bennett and Strehler, 2008). Myo10 may also undergo the kind of self-inhibition exhibited by myosin-VII, wherein part of the tail region folds into and inhibits the motor (Yang et al., 2009) (Figure 1.2). In the mature protein, the neck region is thought to function as a rigid lever arm that amplifies the conformational change in the motor domain, causing the molecule to move a distance proportional to the length of the lever arm, which is typically dictated by the number of IQ motifs in the neck. For example, the 3IQ motifs of Myo10's neck are expected to span ~10 nm, which would allow a Myo10 dimer to potentially reach across ~20 nm in a single step.

The precise structure of the Myo10 lever arm is still unclear due to a recent reanalysis of the ~130 amino acid α-helical region. What was originally predicted to form a dimer-inducing coiled-coil domain is now accepted to be, at least partially, a stable single α-helix (SAH). SAH domains function as stiff extensions of the lever arm and have recently been discovered in several myosins (Baboolal et al., 2009; Sivaramakrishnan et al., 2008). In the case of Myo10, the SAH domain occupies at least

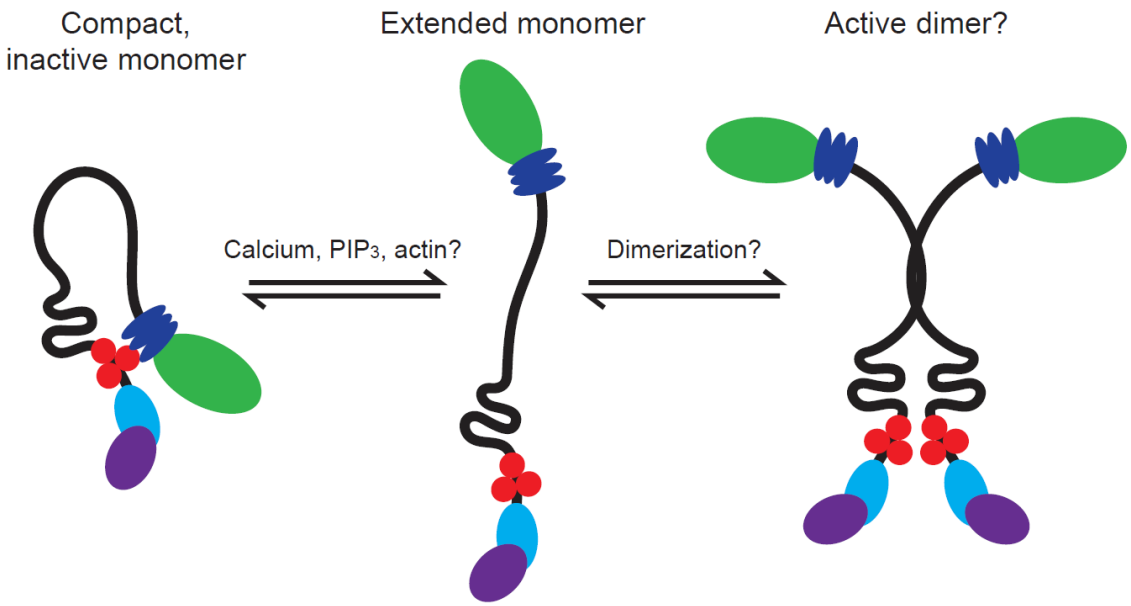

Figure 1.2. Model of possible Myo10 regulation

Myo10's predominant intracellular state may resemble a compact, inactive monomer. Binding to actin by the motor domain, or to other cargos by domains in the tail, may cause the monomer to extend. A final, active dimer may be formed either when the local concentration of extended monomers reaches some threshold, or by binding to specific cargos via the Myo10 tail.

the first 36 of the α-helical region and possibly much more, extending the lever arm and leaving a much shorter region that might form a coiled-coil (Berg et al., 2000; Knight et al., 2005a). The ability of Myo10 to form a dimer has therefore become somewhat controversial.

Whether through the use of a coiled-coil domain or by some other mechanism, Myo10 appears to undergo dimerization under certain circumstances. While electron microscopy revealed that a purified HMM-like Myo10 remained mostly (90%) monomeric, the 10% of the HMM-Myo10 population that successfully formed dimers under these in vitro conditions appeared to have lever arms that were much longer than expected for a neck consisting of only 3IQ motifs. A more recent study by Sun et al. discovered that HMM-Myo10s readily dimerize when brought into proximity, suggesting that the distal portion of the predicted coiled-coil domain retains some dimer-forming ability. To test the necessity of dimerization, many groups have created "forced-dimer" constructs of Myo10 that include a region that artificially induces dimerization. Experiments using different forced-dimer versions of HMM-like Myo10 indicate that the ability to dimerize is necessary for Myo10 to move processively (Kerber et al., 2009; Nagy et al., 2008; Nagy and Rock, 2010; Ricca and Rock, 2010; Sun et al., 2010). Consistent with this theory, a construct containing only the head and neck, thus lacking a coiled-coil domain, is unable to localize to the tips of filopodia (Berg and Cheney, 2002). It is possible that in the environment of the cell, Myo10 is subject to regulated dimerization either through cargo binding, as has been reported for Myosin-VI, or through high local concentrations in the regions of the cell where it accumulates (Iwaki et al., 2006; Park et al., 2006; Phichith et al., 2009; Yu et al., 2009).

Immediately following the α-helical region are three proline-rich PEST regions, which have been implicated as sites of cleavage by calcium-dependent calpain (Berg et al., 2000; Rechsteiner and Rogers, 1996). While cleavage at the PEST sites can occur in vitro, generating an HMM-like Myo10 as well as a tail fragment, it is not yet known whether this is an important process in vivo (Berg et al., 2000). After the PEST regions, the Myo10 tail contains a cluster of three pleckstrin homology (PH) domains in an unusual arrangement; the second PH domain (PH2) is inserted into a putative surface loop of PH1 (Figure 1). The inclusion of PH domains allows Myo10's tail to bind directly to the plasma membrane via phosphatidylinositol phosphates (Berg et al., 2000; Cox et al., 2002; Isakoff et al., 1998; Macias et al., 1994; Musacchio et al., 1993; Tacon et al., 2004; Yonezawa et al., 2003). This membrane-binding ability is unique among the many myosins discovered so far and may lead to an increase in the local concentration of Myo10 to levels that favor dimerization (Sun et al., 2010). Additionally, the presence of PH domains raise the possibility that Myo10 functions downstream of PI3-kinase signaling. Indeed, the PH2 domain of Myo10 is known to function downstream of PI3-kinase in macrophage phagocytosis (Cox et al., 2002) and the inability to bind to PtdIns(3,4,5)P3 shifts Myo10's localization from the plasma membrane to Rab7-positive vesicles (Plantard et al., 2010).

Following the PH domains, the Myo10 tail contains a Myosin Tail Homology 4 (MyTH4) domain, which has been shown to bind to microtubules and may allow Myo10 to act as a link between the actin and microtubule cytoskeletons (Narasimhulu and Reddy, 1998) (Weber et al., 2004). The tail of Myo10 ends in a FERM domain, named after the proteins in which the domain was originally discovered, Band 4.1, Ezrin,

Radixin, and Moesin. Other FERM domain-containing proteins serve to link the actin cytoskeleton to integral membrane proteins (Chishti et al., 1998), and the FERM domain of Myo10 has been shown to bind to the NPXY motif of the cytoplasmic domain of β5 integrin (Zhang et al., 2004). In addition to binding to cargos individually, the MyTH4 and FERM domains can also act in conjunction to bind to some cargo proteins (Wei et al., 2011; Wu et al., 2011). To bind to the netrin receptor, DCC, for example, the formation of a MyTH4/FERM structural supramodule is apparently required. It is also likely, according to structure-based sequence analysis, that all MyTH4/FERM tandems form this supramodule. It will be interesting to see whether this union of the MyTh4 and FERM domains affects their interactions with other binding partners.

Myosin-X localizes to the leading edge of lamellipodia and the tips of filopodia

One of Myo10's most defining characteristics is its striking localization to the tips of the cellular protrusions called filopodia (Figure 1.3). When considering the movement of motors in filopodia, it is important to note the constant retrograde flow of filopodial actin. Against this steady rearward flow, Myo10 uses its own motor force to migrate towards and maintain itself at filopodial tips. As one might expect, the motor domain is necessary for Myo10's tip localization while an HMM-like construct is sufficient (Berg and Cheney, 2002). Although Myo10 is thought to prefer bundled-actin structures, it is also known to localize to the leading edge of lamellipodia, broadening its range to areas of dynamic actin.

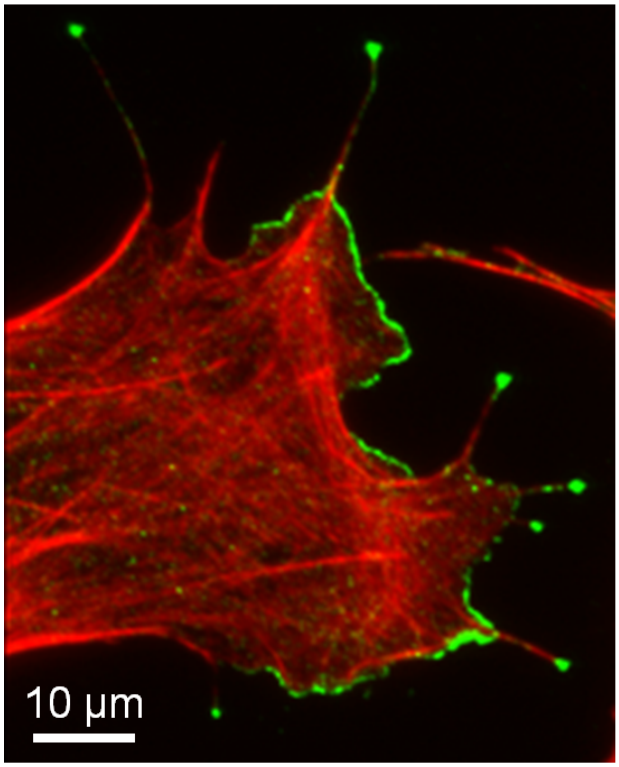

Figure 1.3. Myo10 localizes to filopodial tips and the leading edge of lamellipodia

A bovine aortic endothelial cell fixed and stained with rhodamine-phalloidin (red) and antibodies against My10 (green). Image courtesy of Melinda Divito.

Myosin-X potently induces filopodia

While Myo10 exhibits a clear affinity for filopodia, its functions in these structures have not been completely characterized. There is, however, a large body of evidence indicating that Myo10 is crucial for the formation of filopodia. Overexpression of Myo10 is sufficient to induce a massive increase in both substrate-attached and non-adherent filopodia (Berg and Cheney, 2002) (Figure 1.4). Likewise, knockdown of Myo10 resulted in a dramatic loss of filopodia in HeLa cells. Myo10 may induce substrate-attached filopodia via an integrin-dependent mechanism, causing more filopodia to stick to and become stabilized by the substrate (Zhang et al., 2004). The vast majority of filopodia, however, are non-adherent, and a Myo10 construct that lacks the integrin-binding FERM domain is also capable of inducing filopodia (Bohil et al., 2006). In contrast, an HMM-like construct does not induce filopodia. This evidence indicates that although the tail of Myo10 is required, there may be an integrin-independent mechanism of Myo10's induction of filopodia. One alternate theory proposes that Myo10 can crosslink actin fibers at the leading edge of the lamellipodium, generating actin bundles that could form new filopodia (Tokuo et al., 2007). These models do not exclude the possibility that Myo10 transports some other proteins critical for filopodial formation or maintenance (Ross et al., 2008). Myo10 may perform a similar function in the filopodia-like structures, invadopodia, which are protrusions associated with metastatic cancer cells. Myo10 localizes to the tips of invadopodia and is required for their elongation, suggesting a provocative link between Myo10 and cancer cell metastasis (Schoumacher et al., 2010).

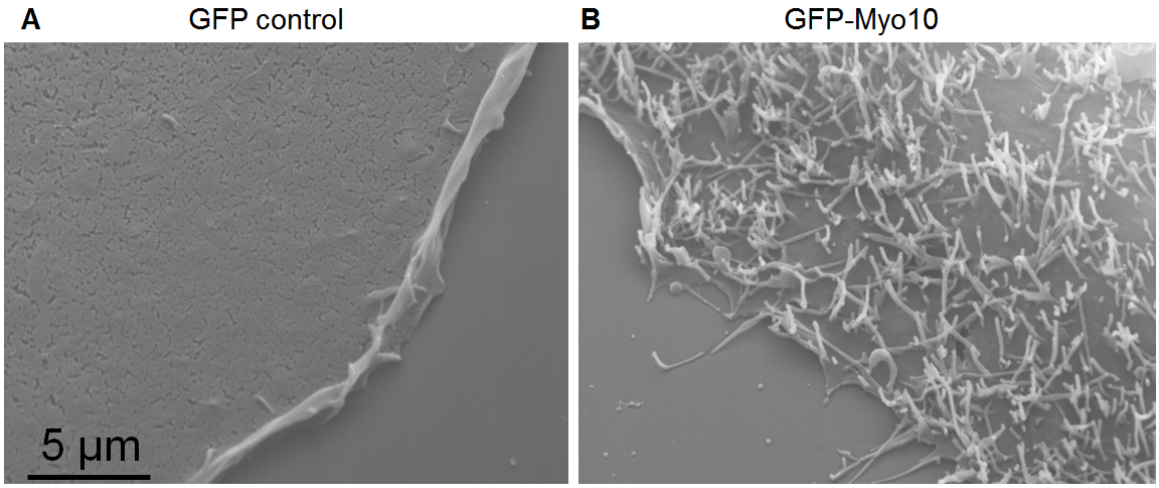

Figure 1.4. Myo10 overexpression induces filopodia formation

Scanning electron micrographs of Cos-7 cells expressing GFP (**A**) or GFP-Myo10 (**B**). Images courtesy of Aparna Bohil.

Myosin-X undergoes intrafilopodial motility

Consistent with the hypothesis that Myo10 propels itself along filopodial actin, GFP-tagged full-length Myo10 constructs have long been known to display striking motility along the filopodia of living cells (Berg and Cheney, 2002) (Figure 1.5). Bright puncta of Myo10 not only localize strongly to filopodial tips, but also move rearwards at rates closely matching those of actin retrograde flow (~15 nm/s). It is thought that these rearward movements represent Myo10 molecules that have coupled to the rearward treadmilling filopodial actin bundle, riding it like packages on a conveyor belt. Occasionally, these Myo10 puncta migrate back towards the tip at ~80 nm/s. More recently, single-molecule microscopy techniques were employed to detect a previously uncharacterized, extremely faint population of Myo10 particles that undergo forward movement at rates that more closely match those exhibited in vitro (~600 nm/s) (Kerber et al., 2009). These fast-forward events can be quite frequent, with new molecules of Myo10 moving up the shaft of an individual filopodium as often as every second. The forward movement of either the large clusters or the single molecules of Myo10 require a functional motor, and an HMM-like construct was found to be sufficient, indicating that in both cases Myo10 is propelling itself. Interestingly, an HMM-Myo10 that included an artificial forced-dimer domain in the α-helical region was also capable of exhibiting fast forward movement at the single-molecule level, indicating that a head, neck, and the ability to dimerize is also sufficient. Although it was not clear from initial "single-molecule" imaging experiments whether the fast, faint particles of Myo10 represented monomers or dimers, a more recent study reported two-step photobleaching of these particles, suggesting that they consist of dimers (Watanabe et al., 2010).

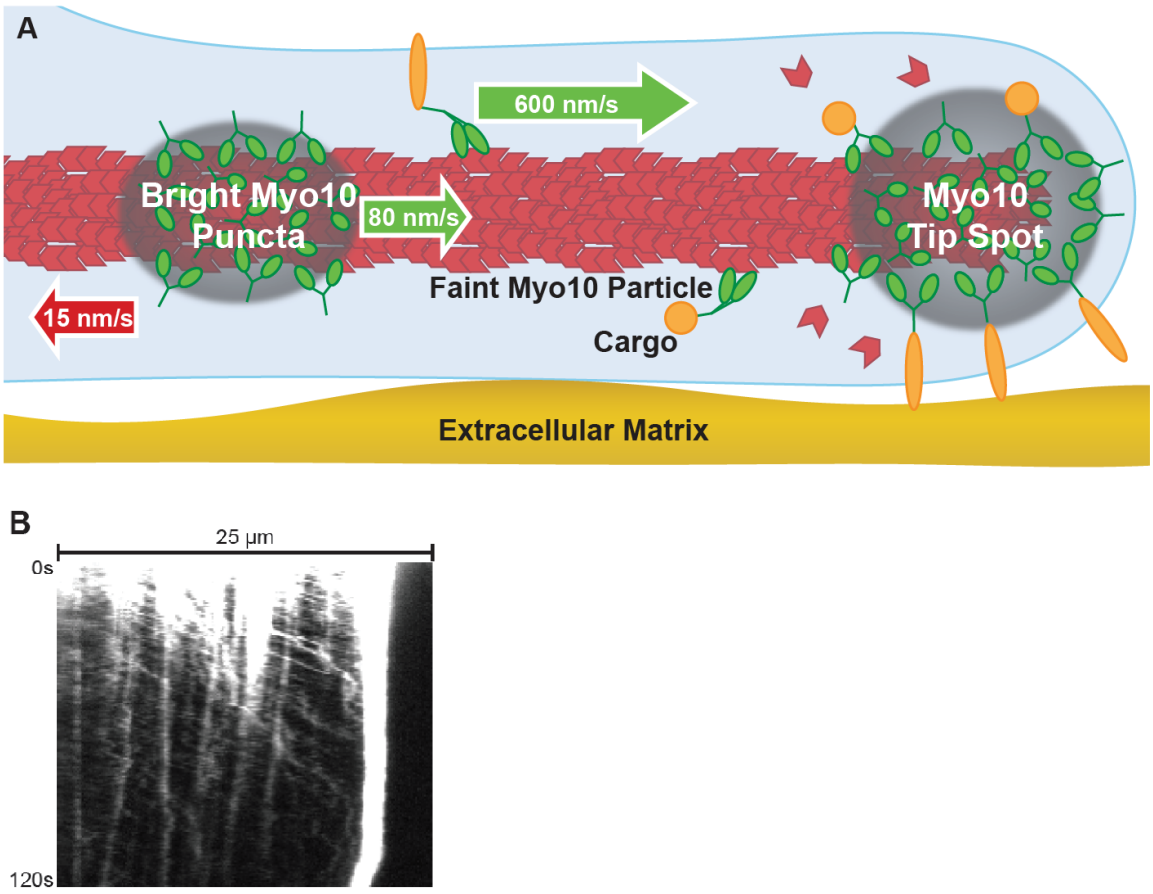

Figure 1.5. Myo10 undergoes intrafilopodial motility

(**A**) Model of Myo10 movement in filopodia. Large clusters of Myo10 (green) are commonly observed both at tips and along the filopodial shaft sliding rearward at ~15 nm/s and migrating forward at ~80 nm/s. These clusters may include as yet undiscovered scaffolding components, actin polymerization machinery, or other cargo (gray). Meanwhile, individual Myo10 monomers or dimers move much faster towards filopodial tips, ~600 nm/s. This highly motile population of Myo10 may also be transporting either cytoplasmic or membrane-associated cargo proteins (orange). (**B**) Kymograph of a filopodium from a HeLa cell transfected with GFP-Myo10 and imaged using single-molecule TIRF. Note the complex juxtaposition of the various modes of Myo10 intrafilopodial motility.

Does Myosin-X transport cargo in filopodia?

Due to its ability to propel itself along filopodial actin, Myo10 is an excellent candidate to act as a cargo delivery motor in a putative, filopodia-specific transport system (Kerber et al., 2009; Nambiar et al., 2010). Consistent with this model, bright puncta of Myo10 have been reported to undergo cotransport with VASP and VE-cadherin in filopodia (Almagro et al., 2010; Tokuo and Ikebe, 2004). It should be noted, however, that it has not yet been shown whether Myo10 is necessary for the transport of its binding partners. These experiments may require the development of Myo10 knockout cell lines. It will also be important in the future to show convincing evidence for Myo10 directly transporting other proteins, a feat that may require more sensitive single-molecule techniques than those employed so far.

Filopodia are also known to serve as passageways for the transport of cargo between cells. For example, melanosomes are pigment-producing organelles that appear to be delivered from melanocytes to keratinocytes along filopodia in a process thought to be driven by myosin-Va (Scott et al., 2002). A recent study, however, demonstrated the importance of Myo10 in this transport system. Knockdown of Myo10 in either the melanocytes or the keratinocytes resulted in inhibition of melanin uptake while ultraviolet light upregulated both melanosome transfer and Myo10 expression (Singh et al., 2010). Intriguingly, a similar filopodial transport system may also be exploited by retroviruses to infect neighboring cells, although the contribution of Myo10 in this process has not yet been investigated (Lehmann et al., 2005; Sherer et al., 2007; Sherer and Mothes, 2008).

Myosin-X is required for endothelial cell migration and junction formation

In addition to acting as transport routes for intracellular cargos, filopodia are also thought to be crucial for signaling and cellular migration. Interestingly, BMP6-dependent filopodial extension and, consequently, directional migration in endothelial cells requires Myo10 (Pi et al., 2007). In this process, Myo10 serves as a necessary part of the signaling pathway that allows the cell to detect BMP6 in the extracellular environment, possibly by transporting the BMP6-receptor ALK6 to filopodial tips. Endothelial cell filopodia play an important role in establishing cell-cell junctions, which are held together by a cell-cell adhesive receptor, VE-Cadherin. VE-Cadherin was recently reported to immunoprecipitate with Myo10 and undergo coordinate movement with Myo10 in endothelial cell filopodia. Importantly, expressing a putative dominant negative Myo10 construct, consisting of the Myo10 FERM domain, inhibited the localization of VE-Cadherin (Almagro et al., 2010).

Myosin-X is required for spindle assembly and orientation

In addition to its clear association with filopodia-like structures, Myo10 is also important in a process that has little in common with cellular protrusions: mitotic spindle orientation. Assembly of the mitotic spindle and anchoring of the nucleus in Xenopus laevis oocytes are disrupted when Myo10 function is presumably inhibited by either anti-Myo10 antibodies or a Myo10-tail construct (Weber et al., 2004). More dramatically, the use of morpholinos to inhibit Myo10 expression in developing embryos results in multipolar spindles (Woolner et al., 2008) (Figure 1.6). Proper orientation of the mitotic spindle is also dependent on Myo10. HeLa cells, which normally orient their mitotic

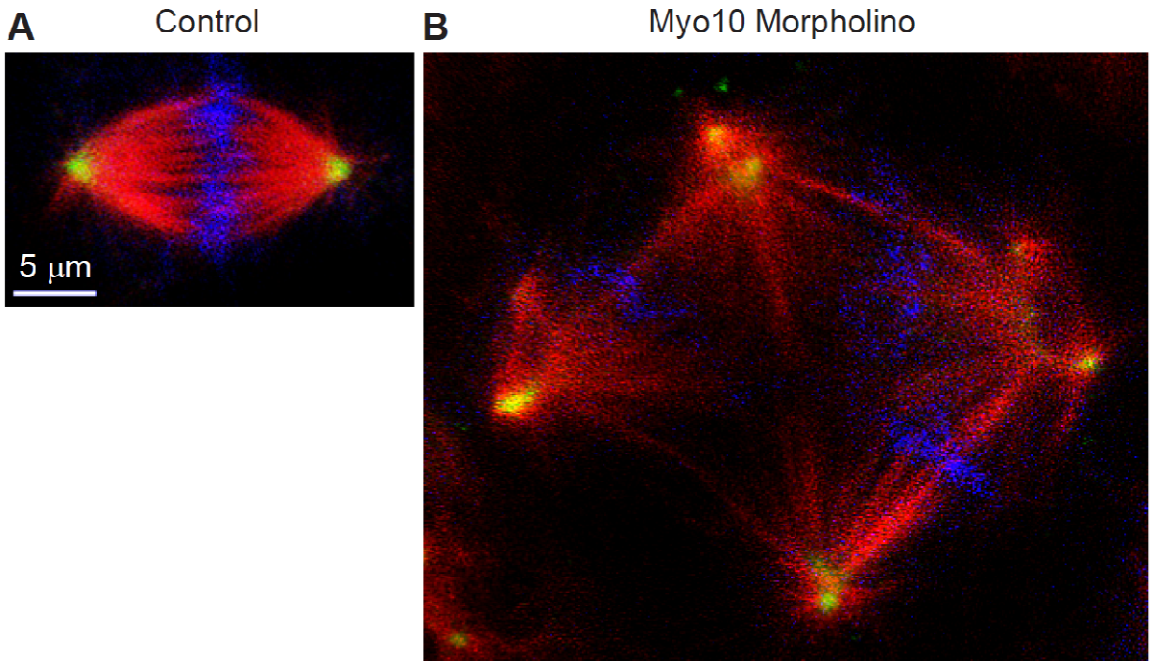

Figure 1.6. Knockdown of Myo10 results in the formation of multipolar spindles

(**A**) Control or (**B**) Myo10 morpholino-treated cells of a Xenopus embryo. Cells were fixed and stained for β-tubulin (red), γ-tubulin (green), and DNA (blue). Image courtesy of Bill Bement.

spindles parallel to the substrate in an integrin-mediated, substrate-dependent manner, lose the ability to correctly orient their spindles when Myo10 expression is knocked down with siRNA (Toyoshima and Nishida, 2007). Knockdown of Myo10 also increases the probability of the cancer cell line MDA231 to produce multipolar spindles (Kwon et al., 2008). It is hypothesized that Myo10 links the spindle-associated F-actin with astral microtubules and applies a contractile force to the spindle, counteracting the stretching force applied by cortical F-actin (Wuhr et al., 2008).

Myosin-X is important for axon outgrowth

While most tissues express full-length Myo10, expression in the mouse brain peaks during the first week after birth, which is also the period of peak synapse formation. Myo10 expression then plummets in the adult mouse brain, but the brain also expresses an enigmatic isoform that lacks the motor domain (Sousa et al., 2006). This "headless" isoform is otherwise intact and may represent a naturally occurring dominant negative. Indeed, expressing a headless Myo10 construct inhibits the migration of neuronal cells in vitro (Wang et al., 2009) and impairs chick commissural neuron axon projection in vivo (Zhu et al., 2007). In neurons, actin and microtubules are both important for axon guidance and extension, with filopodia being especially important for axonal path-finding (Dent and Gertler, 2003). Cortical neurons from a mouse line lacking the three Ena/VASP proteins, Mena, VASP, and EVL, do not form filopodia or generate neurites. Expressing Myo10 in these triple knockout cells rescues filopodia formation and neuritogenesis (Dent et al., 2007). Interestingly, Myo10 is upregulated ~7-fold following nerve injury, perhaps due to the reactivation of signaling pathways

normally active during development. In development, axon path-finding is regulated by a group of proteins called Netrins, whose receptors include Deleted in Colorectal Cancer (DCC). DCC localizes to neurite tips in a Myo10-dependent manner and also induces Myo10-dependent filopodia formation and elongation (Zhu et al., 2007). Together, these data strongly indicate a developmentally critical role for Myo10 in axon outgrowth.

Myosin-X is required during development for neural crest cell migration

Although there is currently no knockout animal model for Myo10, exciting studies using Xenopus laevis reveal that Myo10 is required for the proper migration of cranial neural crest cells (Hwang et al., 2009) (Nie et al., 2009). Neural crest cells are multipotent, migratory cells that give rise to several cell types including craniofacial cartilage and bone, melanocytes, and peripheral neurons (Huang and Saint-Jeannet, 2004). In the Xenopus embryo, Myo10 is predominantly expressed in the neural crest cells in the premigratory and migratory stages. Knocking down Myo10 expression with morpholinos causes a loss of neural crest cell migration and results in a dramatic decrease in the size of the cranium. The loss of migration can be rescued in vitro by expressing exogenous Myo10, confirming that the phenotype is due to the loss of Myo10. This defect in cell migration appears to be caused by inhibited cellular adhesion and polarization of the neural crest cells. It will be important to learn whether Myo10 proves to be required in other migratory cell types and other developmental processes.

How does Myosin-X select for filopodial actin?

Much of Myo10's filopodia-centric functions rely on its ability to preferentially localize to bundled actin. Recent advances in the understanding of Myo10's biophysical properties are steadily revealing the mechanism underlying Myo10s affinity for bundled actin in the cell. One hypothesis proposes that Myo10 binds favorably to bundled actin because its lever arms possess the distinct length and flexibility to endow the myosin with the unique ability to bind each motor domain to separate, neighboring actin filaments. In a series of experiments from the Rock group, Myo10 has been shown to initiate longer, more frequent runs on bundled actin than filamentous actin, and that Fascin, the filopodial actin bundler, is required for proper Myo10 localization in vivo (Nagy et al., 2008). Myo10 also appears to prefer parallel actin bundles in ex vivo systems in which the stabilized cytoskeletons of fixed, detergent-treated cells are used to seed purified motors (Brawley and Rock, 2009). The specifics of Myo10's behavior on bundled and filamentous actin remain unclear, with reported step-sizes ranging from 18 nm to 34 nm (Ricca and Rock, 2010; Sun et al., 2010). There is also disagreement regarding whether Myo10 spirals in a right-handed, left-handed, or unbiased fashion on filaments and bundles. Domain-swapping experiments indicate that Myo10's bundle selectivity, however, appears to rely on the properties of its α-helical region and may involve the amount of flexibility that the region lends to Myo10's lever arm (Nagy and Rock, 2010). Much of the discrepancies may be due to differences in the constructs used by different groups. Some forced-dimer constructs may alter the flexibility of the α-helical region or may place them out of register. It is clear from these studies that the field would benefit

greatly from a purified, full-length version of Myo10 that could be used to establish the step size, processivity, and bundle selectivity of the native protein.

Discussion

Although Myo10's provocative localization to filopodia and similar structures has long hinted at importance in development, the first confirmation of its role in vivo has only recently come to light. The requirement for Myo10 in neural crest cell migration may represent only the first of many potential roles in development, considering its importance in other in vitro systems (e.g. endothelial cell migration and mitotic spindle formation). The creation of true knockout animal models may reveal other developmental processes that require Myo10. Cell lines that truly lack Myo10 would also provide invaluable new testing grounds to more fully characterize its role in the cell.

Indeed, Myo10 has yet to be fully characterized at the molecular level and many questions persist. How is Myo10 regulated? Does it dimerize? Does it transport cargo? Although great progress has been made using various truncated and forced-dimer versions of Myo10, the field would benefit greatly from a purified full-length Myo10 that could be used for biophysical studies. Likewise, much has been learned from in vitro and ex vivo systems, but in vivo approaches may be required to tease apart the actual dimerization status, step size, and bundled actin behavior that Myo10 exhibits in the cell. A better understanding of Myo10's molecular characteristics will undoubtedly lead to a better understanding of its role in the broader context of human health and disease.

Chapter 2: Imaging Myosin-X at the Single-Molecule Level Reveals a Novel Form of Motility in Filopodia

Michael L. Kerber, Damon T. Jacobs, Luke Campagnola, Brian D. Dunn, Taofei Yin,

Aurea D. Sousa, Omar A. Quintero, and Richard E. Cheney

Summary

Although many proteins, receptors, and viruses are transported rearward along filopodia by retrograde actin flow (Hu et al., 2007; Lidke et al., 2005; Sherer et al., 2007), it is less clear how molecules move forward in filopodia. Myosin-X (Myo10) is an actin-based motor hypothesized to use its motor activity to move forward along actin filaments to the tips of filopodia (Berg and Cheney, 2002). Here we use a sensitive total internal reflection fluorescence (TIRF) microscopy system to directly visualize the movements of GFP-Myo10. This reveals a novel form of motility at or near the single-molecule level in living cells wherein extremely faint particles of Myo10 move in a rapid and directed fashion towards the filopodial tip. These fast forward movements occur at ~600 nm/s over distances of up to ~10 um and require Myo10 motor activity and actin filaments. As expected for imaging at the single-molecule level, the faint particles of GFP-Myo10 are diffraction-limited, have an intensity range similar to single GFP molecules, and exhibit

stepwise bleaching. Faint particles of GFP-Myo5a can also move towards the filopodial tip, but at a slower characteristic velocity of ~250 nm/s. Similar movements were not detected with GFP-Myo1a, indicating that not all myosins are capable of intrafilopodial motility. These data indicate the existence of a novel system of long-range transport based on the rapid movement of myosin molecules along filopodial actin filaments.

Results and Discussion

Filopodia are slender actin-based extensions thought to function as cellular sensors in processes such as nerve growth and blood vessel development. Filopodia have a relatively simple structure consisting of a bundle of parallel actin filaments surrounded by the plasma membrane (Mattila and Lappalainen, 2008; Wood and Martin, 2002). Each actin filament has its barbed end oriented towards the tip of the filopodium, and actin monomers are constantly added to the filament at its barbed end. The actin in filopodia typically moves rearward at rates of 10-100 nm/s in a process known as retrograde flow. Although retrograde flow (Albrecht-Buehler and Goldman, 1976) is now known to be powered by a combination of actin polymerization and myosin-II mediated contraction (Medeiros et al., 2006), the mechanisms by which molecules move forward in filopodia are much less clear. Since microtubules and membranous vesicles are generally absent from filopodia, forward movement in filopodia is likely to depend either on diffusion or an actin-based mechanism.

Myo10 is an actin-based motor protein that localizes to the tips of filopodia and has potent filopodia-inducing activity (Bohil et al., 2006; Sousa and Cheney, 2005). The

Myo10 heavy chain consists of a myosin head domain responsible for force production, a neck domain that provides binding sites for calmodulin or calmodulin-like light chains (Rogers and Strehler, 2001), and a large tail (Sousa and Cheney, 2005). The tail includes a segment that was initially predicted to form a coiled coil (Berg et al., 2000), 3 PH domains that can bind to inositol phospholipids such as PIP_3 (Mashanov et al., 2004), a MyTH4 domain that can bind to microtubules (Weber et al., 2004), and a FERM domain that can bind to candidate cargoes such as β-integrins (Zhang et al., 2004). Imaging with conventional epifluorescence revealed that the bright puncta of GFP-Myo10 normally present at the tips of filopodia sometimes vacate the tip and move slowly rearward at 10-20 nm/s (Berg and Cheney, 2002), the rate of retrograde actin flow in HeLa filopodia. Bright puncta also occasionally moved forward at ~80 nm/s, leading to the hypothesis that Myo10 moves forward by using its barbed-end motor activity to transport itself along filopodial actin filaments and that it moves rearward by binding in a rigor-like state to actin filaments undergoing retrograde flow. Consistent with this, a Myo10 construct comprised only of the head, neck, and predicted coiled coil (Myo10-HMM) was sufficient for tip localization (Berg and Cheney, 2002). Although a baculovirus-expressed Myo10-HMM-like construct appears largely monomeric *in vitro* (Knight et al., 2005b), induced dimerization of Myo10 head-neck constructs leads to tip localization *in vivo* (Tokuo et al., 2007). Kinetic analyses of Myo10 head-neck constructs indicate they have duty ratios intermediate between those of highly processive motors such as Myo5a, and non-processive motors, such as muscle myosin (Homma and Ikebe, 2005; Kovacs et al., 2005). Most importantly, recent single-molecule experiments using *in vitro* motility

assays show that a HMM-like Myo10 forced-dimer can move rapidly and processively on artificial actin bundles at 340-780 nm/s (Nagy et al., 2008).

Although *in vitro* experiments at the single-molecule level have led to many fundamental insights about motor proteins, tracking the movements of individual motor molecules *in vivo* has remained a major challenge. To test whether cells exhibit robust but previously unsuspected forms of trafficking at the single-molecule level, here we use TIRF to image the movements of GFP-tagged motor proteins in the filopodia of living cells. The TIRF system used here provides approximately an order of magnitude increase in sensitivity and temporal resolution compared to previous conventional fluorescence microscopy (Berg and Cheney, 2002) while the linear organization and defined polarity of filopodia greatly facilitates particle tracking and analysis. In addition, the ~100 nm thickness of a filopodium means that all or most of a filopodium will be within the 100-200 nm penetration distance of the TIRF field. Imaging substrate-attached filopodia with TIRF thus provides a system that has much of the simplicity of an *in vitro* motility assay, but in the context of a living cell.

TIRF reveals a novel form of rapid motility in filopodia

To test the sensitivity of our TIRF system, we adsorbed low concentrations of pure GFP onto coverslips and imaged with TIRF. As expected for single-molecule imaging of GFP (Pierce et al., 1997), this resulted in the detection of faint spots that were diffraction-limited, underwent stepwise bleaching, and exhibited "blinking" (Movie S1). When living HeLa cells were transiently transfected with full-length GFP-Myo10 and

imaged by TIRF under the same conditions, bright labeling was observed at the tips of filopodia as well as at the ventral surface of the cell (Movie S2). Most importantly, close inspection of individual filopodia revealed a novel form of movement in which extremely faint particles of GFP-Myo10 moved rapidly towards the tip (Movies S3-S4).

The movements of the faint particles along a given filopodium are clearly illustrated in kymographs, which reveal numerous faint tracks corresponding to the rapid and directed movements of faint particles of GFP-Myo10 towards the tip (Figures 2.1 and 2.2). Approximately a dozen such tracks are visible in the 40 s time-lapse illustrated in Figure 2.1B. Tracks from these fast forward movements appeared to have relatively constant intensities and most traveled the entire ~5 µm length of the filopodium. Although most particles moved in a smooth and apparently processive fashion until they reached the filopodial tip, particles occasionally paused or transiently reversed, generating Z-shaped tracks (Figures 2.1D and 2.2). Rapid forward movements of faint Myo10 particles were detected under a variety of TIRF imaging conditions, including the use of different camera settings, different magnifications, and a different TIRF illuminator (Figure 2.2). At 25° C, the faint particles of Myo10 moved forward at an average velocity of 578 ± 174 nm/s (Figure 2.1E). At 37° C the particles moved faster (840 ± 210 nm/s), as expected for a motor-driven biological process. The velocities of GFP-Myo10 particles detected here in living cells are quite similar to the 340-780 nm/s reported for movements of individual molecules of a Myo10 forced-dimer on artificial actin bundles (Nagy et al., 2008). The forward movements detected here by TIRF are clearly distinct from the relatively infrequent forward movements of bright GFP-Myo10

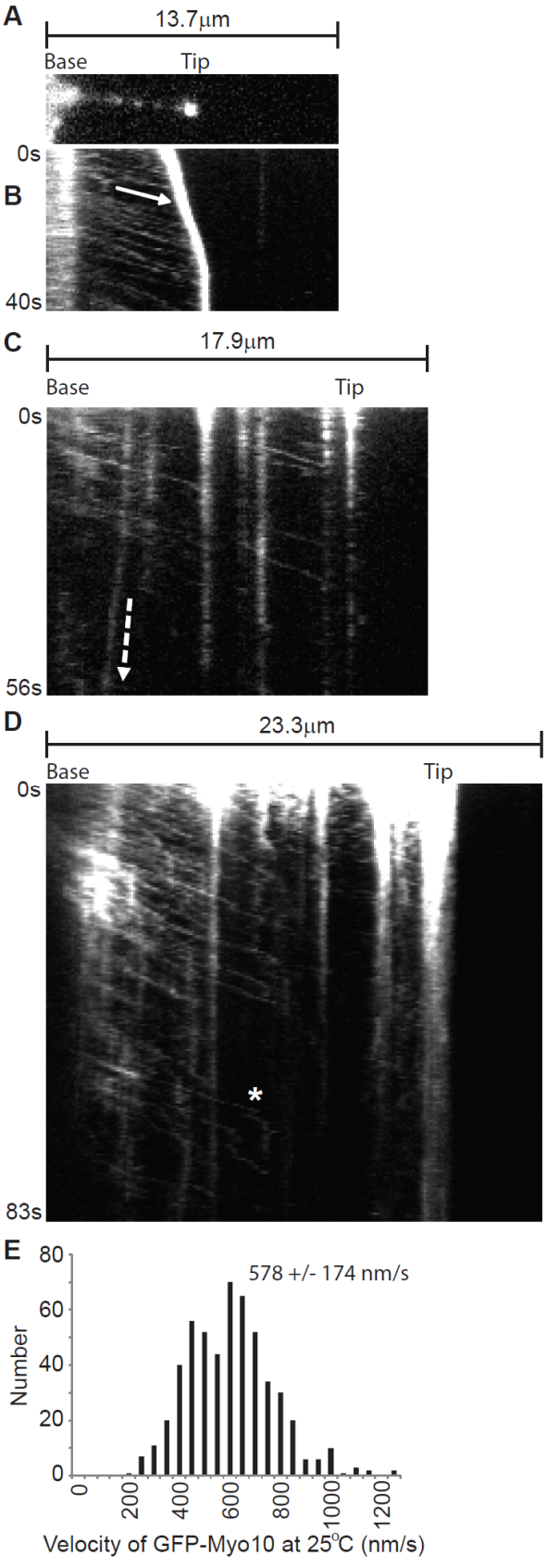
A
13.7μm
Base
Tip
0s
B
40s
C
17.9μm
Base
Tip
0s
56s
D
23.3μm
Base
Tip
0s
*
83s
E
578 +/- 174 nm/s
Number
80
60
40
20
0
0
200
400
600
800
1000
1200
Velocity of GFP-Myo10 at 25°C (nm/s)

Figure 7.1. TIRF microscopy reveals fast forward movements of faint particles of GFP-Myo10 in living cells

(**A**) TIRF image of a single filopodium from a HeLa cell expressing GFP-Myo10 showing a bright punctum of GFP-Myo10 at the tip of the filopodium, several faint particles of GFP-Myo10 along the shaft, and diffuse fluorescence at the base of the filopodium (See Movie S3). (**B**) Kymograph generated from time-lapse imaging of the same filopodium revealing numerous faint tracks (arrow) sloping gently down to the right that correspond to rapid movements of faint particles towards the tip. The very bright track corresponds to the tip of the filopodium, which was initially extending forward at ~100 nm/s and then stopped. The faint vertical track beyond the tip corresponds to a faint particle of fluorescent debris. (**C**) Kymograph from a branched retraction fiber in a HeLa cell stably expressing GFP-Myo10. This kymograph shows faint tracks from fast forward movements as well as vertical tracks from stationary particles. One track slopes steeply down to the left and corresponds to GFP-Myo10 that was moving slowly rearward (dashed arrow). (**D**) Kymograph from a HeLa cell expressing GFP-Myo10 showing numerous faint tracks that terminate midway along a filopodium. One particle moved rapidly forward, transiently reversed, stopped for a few seconds, and then disappeared suddenly (track marked by an asterisk). (**E**) Velocity histogram for fast forward movements of faint GFP-Myo10 particles (531 measurements from 65 filopodia).

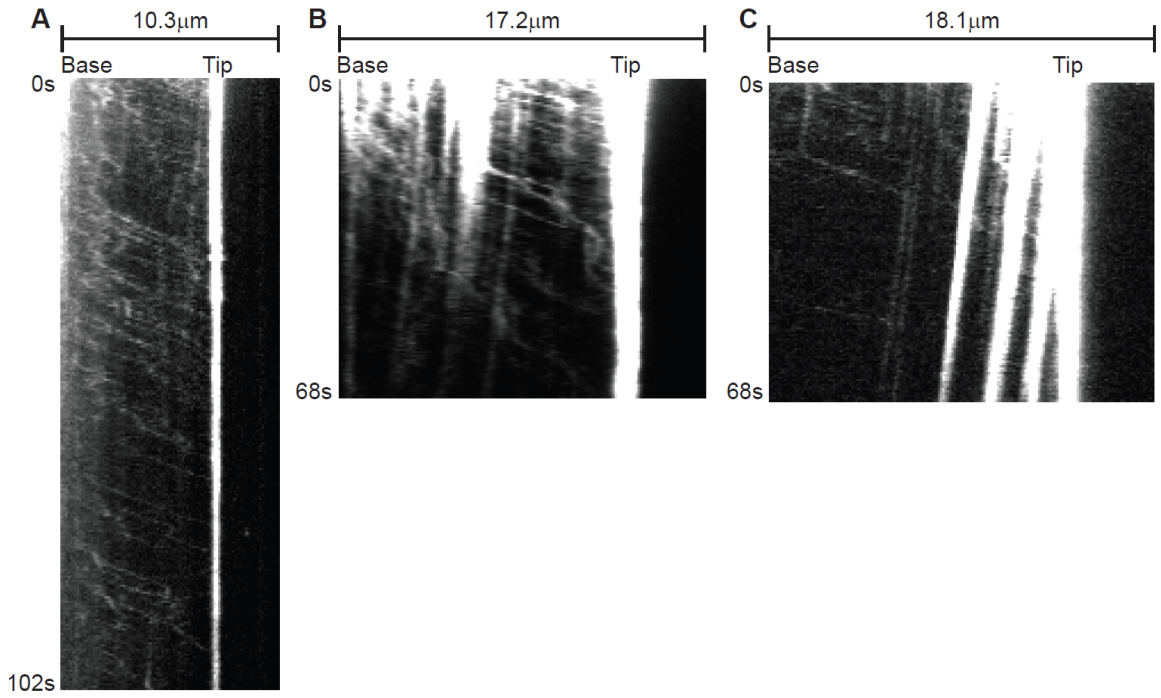

Figure 2.2. Dynamics of GFP-Myo10 in living HeLa cells imaged with TIRF

(A) Kymograph of a filopodium imaged at 37° C using a 60x lens, 1.5x tube lens, 2x2 binning, camera set to maximum gain, a pixel size of 142 nm, and a Nikon TIRF II illuminator. Numerous faint tracks slope gradually down to the right, corresponding to fast forward movements of faint particles of GFP-Myo10. Although most particles move at a relatively constant velocity from base to tip, a few particles appeared to slow down as they approached the tip and others appear to transiently reverse direction, creating Z-shaped tracks. Note that the particles move so rapidly that most reach the tip prior to bleaching, even at full laser power. (**B**) Kymograph of a filopodium imaged using standard imaging conditions (25° C, 60x, 1x tube lens, no binning, zero gain, and a pixel size of 107 nm) except that a Nikon single-molecule TIRF illuminator was used. This kymograph illustrates several different states that Myo10 can exist in, including stationary (vertical lines), moving rapidly forward (tracks that slope gradually down to the right), and moving slowly rearward (tracks that slope steeply down to the left). (**C**) Kymograph of a filopodium imaged under standard conditions with a Nikon TIRF II illuminator. In this filopodium much of GFP-Myo10 was moving slowly rearward.

puncta detected previously by conventional fluorescence in that the particles detected here are much fainter, move 5-10 fold faster, and move forward much more frequently.

In addition to the fast forward movements of faint particles of Myo10, we also detected slow rearward movements (Figure 2.1C and 2.2). The average rate of the rearward movements was 23 ± 8 nm/s (137 measurements from 20 filopodia), a velocity consistent with the hypothesis that GFP-Myo10 moves rearward by binding to actin filaments undergoing retrograde flow. The bright puncta of GFP-Myo10 at the tips of filopodia were generally stationary and thus generated bright vertical tracks that grew gradually dimmer due to photobleaching. Vertical tracks were also sometimes present at different points along a filopodium, indicating that some Myo10 within the filopodial shaft is stationary, perhaps due to association with integrin-based adhesions (Zhang et al., 2004).

It should be noted that we observed obvious movement of Myo10 particles in slender extensions that extended forward during imaging and that would thus be functionally defined as filopodia (Figure 2.1A-B). We also observed similar movements in slender extensions that had the branched morphology of retraction fibers (Figure 2.1C). Since Myo10 particles exhibited the same kinds of motility in both forms of slender extension and both forms of extension contained filopodial markers such as F-actin and the actin bundling protein, fascin (Figure 2.3), we use the convention of Svitkina et al. and refer to these slender extensions collectively as filopodia (Svitkina et al., 2003).

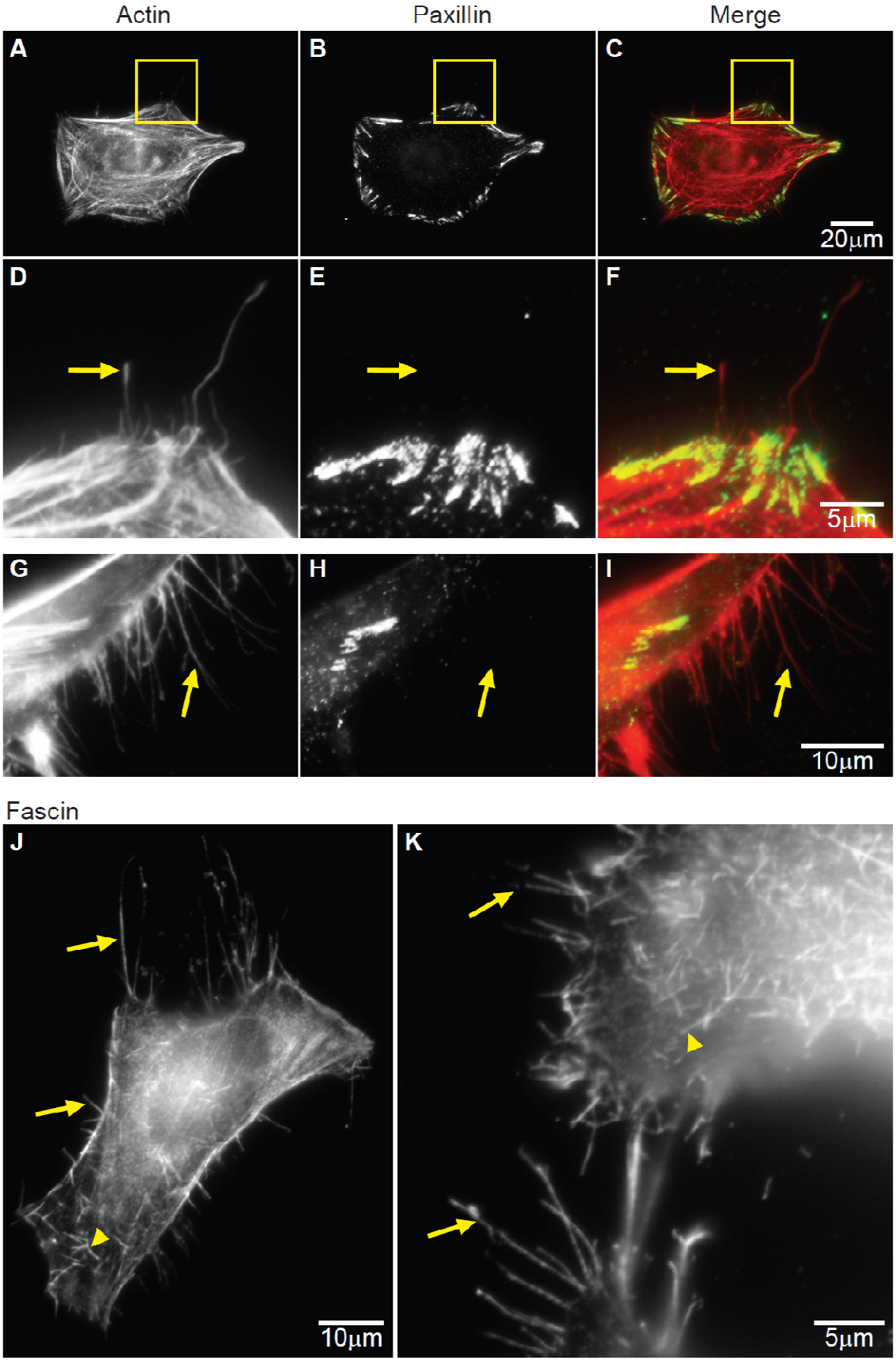
Actin
Paxillin
Merge
A
B
C
20μm
D
E
F
5μm
G
H
I
10μm
Fascin
J
K
10μm
5μm

Figure 2.3. Substrate-attached cell extensions in HeLa cells contain the filopodial markers F-actin and fascin

(**A-C**) A HeLa cell fixed with paraformaldehyde and stained with Alexa 568-phalloidin and an antibody against human paxillin (BD Transduction 611724). (**D-F**) Insets from A-C showing that extensions contain F-actin, but lack detectable levels of the focal adhesion marker, paxillin. (**G-I**) Higher magnification view of an identically fixed and stained HeLa cell with several long, branched extensions. Note that these extensions also contain actin and lack detectable paxillin. (J) A HeLa cell fixed with methanol and labeled with an antibody against human fascin (Dako 55K-2). Note that this filopodial marker labels both cell-surface filopodia as well as substrate-attached cell extensions. (**K**) Higher magnification of another HeLa cell fixed with methanol and stained with human fascin antibody, showing clear labeling of surface filopodia as well as long, substrate-attached cell extensions. Arrow heads indicate filopodia on the cell surface while arrows indicate substrate-attached filopodia and retraction fibers (as defined by branched morphology).

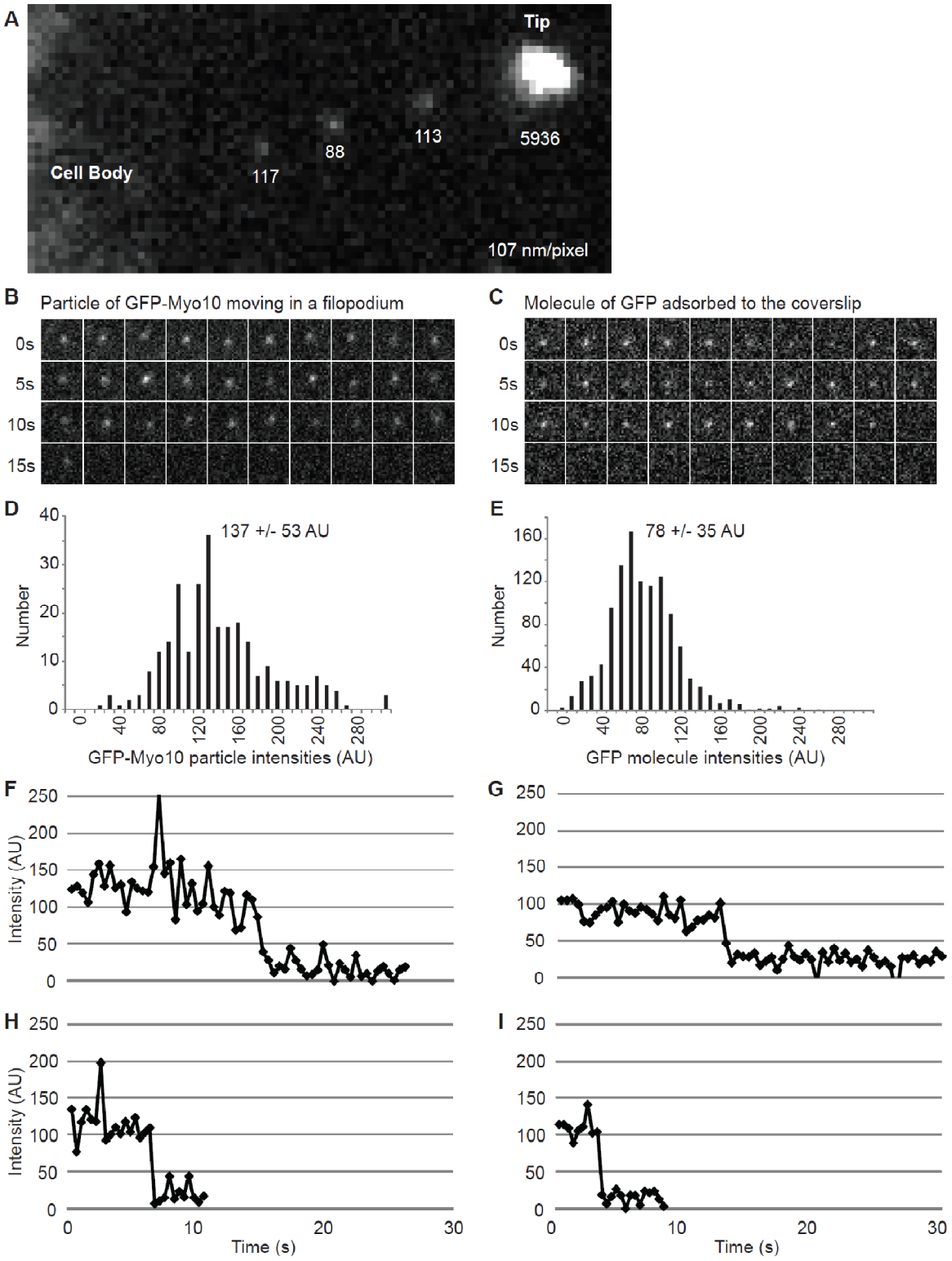
A
Tip
Cell Body
117
88
113
5936
107 nm/pixel
B
Particle of GFP-Myo10 moving in a filopodium
0s
5s
10s
15s
C
Molecule of GFP adsorbed to the coverslip
0s
5s
10s
15s
D
137 +/- 53 AU
Number
GFP-Myo10 particle intensities (AU)
E
78 +/- 35 AU
Number
GFP molecule intensities (AU)
F
Intensity (AU)
G
H
Intensity (AU)
Time (s)
I
Time (s)

Figure 2.4. Faint particles of GFP-Myo10 exhibit characteristics of single molecules

(**A**) High magnification TIRF image of a filopodium showing a bright punctum of GFP-Myo10 at the tip and the diffraction limited nature of 3 faint particles within the filopodial shaft. The numbers indicate the background-corrected, integrated intensity for each spot. (**B**) Images from Kymotracker showing a single faint particle of GFP-Myo10 as it moved rapidly toward the tip of a filopodium and an apparent bleaching event at ~15 s. (**C**) Images from Kymotracker showing a single molecule of GFP adsorbed to a coverslip and an apparent bleaching event. (**D**) Intensity histogram of faint particles of GFP-Myo10 moving rapidly forward in filopodia (268 measurements from 8 filopodia). (**E**) Intensity histogram of single molecules of GFP adsorbed to coverslip surface (1124 measurements). (**F**, **H**) Intensity-versus-time plots from Kymotracker for single particles of GFP-Myo10 that underwent apparent bleaching events as they moved rapidly forward in filopodia. Note that each particle disappeared in a single step rather than gradually fading away. (**G**, **I**) Intensity-versus-time plots from Kymotracker for single molecules of GFP adsorbed on a coverslip.

Faint Myo10 particles have single-molecule characteristics

We next investigated whether the faint particles detected by TIRF exhibited properties expected of single molecules (Mashanov et al., 2004; Pierce et al., 1997). High-magnification views show that the faint particles moving within filopodia are approximately the size expected for a diffraction-limited spot (~0.2 μm at half maximum intensity), whereas the bright puncta at filopodial tips are generally much larger (Figure 2.4). Manual measurements indicated that the faint particles had integrated intensities of ~100 arbitrary units (AU), which is approximately $1/10^{th}$ to $1/100^{th}$ the intensity of a typical tip punctum. To facilitate particle tracking and quantification, we wrote a program called Kymotracker, which utilizes the position and time coordinates from a line on a kymograph to semi-automatically track a particle and measure its intensity through time. As can be seen from the Kymotracker images of a faint particle of GFP-Myo10 as it moves along a filopodium, the faint particles appear diffraction-limited and exhibit relatively constant intensities as they move (Figure 2.4B). In some cases, a particle that had been tracked through several frames disappeared suddenly, as would be expected for photobleaching of a single GFP. Using Kymotracker, the average intensity of the faint particles of GFP-Myo10 in filopodia was found to be 137 ± 53 AU. The intensities of single GFP molecules adsorbed to coverslips and imaged under the same illumination and exposure conditions had a similar magnitude and an overlapping distribution (78 ± 35 AU) (Figure 2.4D-E), although it should be noted that the pure GFP was imaged in TBS rather than cytoplasm. Plots of intensity versus time revealed apparent stepwise bleaching events both for pure GFP on coverslips and for the faint particles moving within filopodia (Figure 2.4F-I). Together these experiments demonstrate that the TIRF

system used here can detect single molecules of pure GFP and that the faint particles of GFP-Myo10 detected in living cells correspond to single molecules or small oligomers.

Particle movements require the Myo10 motor and actin

To investigate the mechanisms responsible for the rapid movement of Myo10, we utilized a panel of Myo10 deletion constructs. No rapid particle movements and no tip localization was detected in HeLa cells transfected with GFP-Myo10-headless, a naturally occurring form of Myo10 that lacks most of the motor domain and thus lacks motor activity (Sousa and Cheney, 2005) (Figure 2.5A). In addition, no rapid forward tracks were detected with a full-length Myo10 construct containing a point mutation in its motor domain that corresponds to a weak actin-binding mutation in other myosins(Friedman et al., 1998) (GFP-Myo10-E456K; Figure 2.6). GFP-Myo10-HMM, which consists of the Myo10 motor, neck, and predicted coiled coil, did undergo rapid particle movements similar to those of full-length Myo10 (Figure 2.5B). This suggests that a dimerized Myo10 head-neck domain is sufficient for fast forward movements. Since systematic analysis of deletion constructs indicated that a forced-dimer construct consisting of the Myo10 head, neck, and first 34 amino acids of the "coiled coil" fused to a GCN4 dimerization domain was the minimal construct able to clearly localize to filopodial tips, we imaged the forced dimer by TIRF and found that it was also capable of fast forward movements in filopodia (Figure 2.6). Together these experiments indicate that rapid movements of faint particles in filopodia require Myo10 motor activity and that

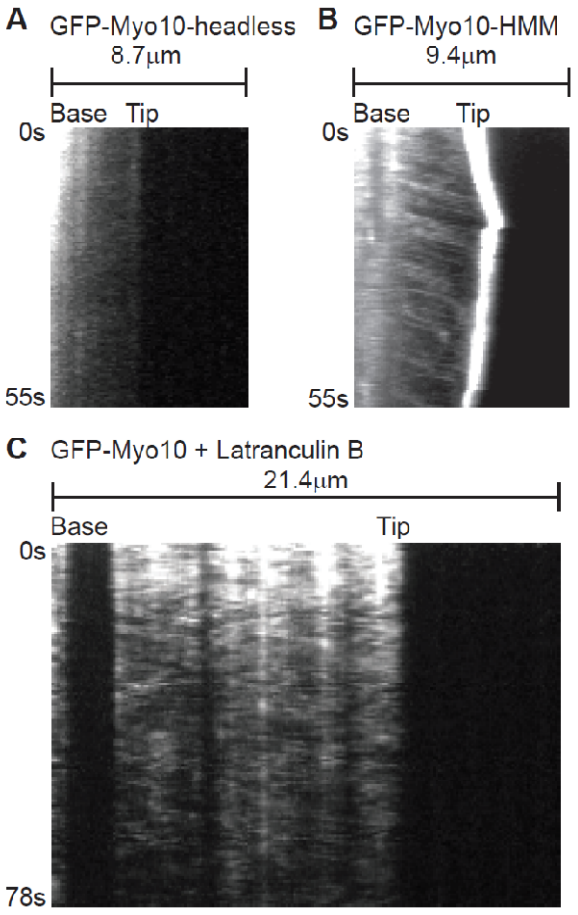

Figure 2.5. Fast Forward movements require the Myo10 motor domain and are inhibited by latrunculin B

(**A**) Kymograph from TIRF imaging of GFP-Myo10-headless in a filopodium. This construct lacks most of the Myo10 motor domain and does not localize to filopodial tips or exhibit obvious fast forward movements. (**B**) Kymograph from TIRF imaging of GFP-Myo10-HMM. GFP-Myo10-HMM is sufficient for tip localization and faint particles of it undergo fast forward movements. (**C**) Kymograph showing that fast forward movements of GFP-Myo10 are blocked by latrunculin B. Cells were treated with 1 μM latrunculin B for ~10 minutes to depolymerize actin filaments and the remaining, substrate-attached filopodia were imaged by TIRF.

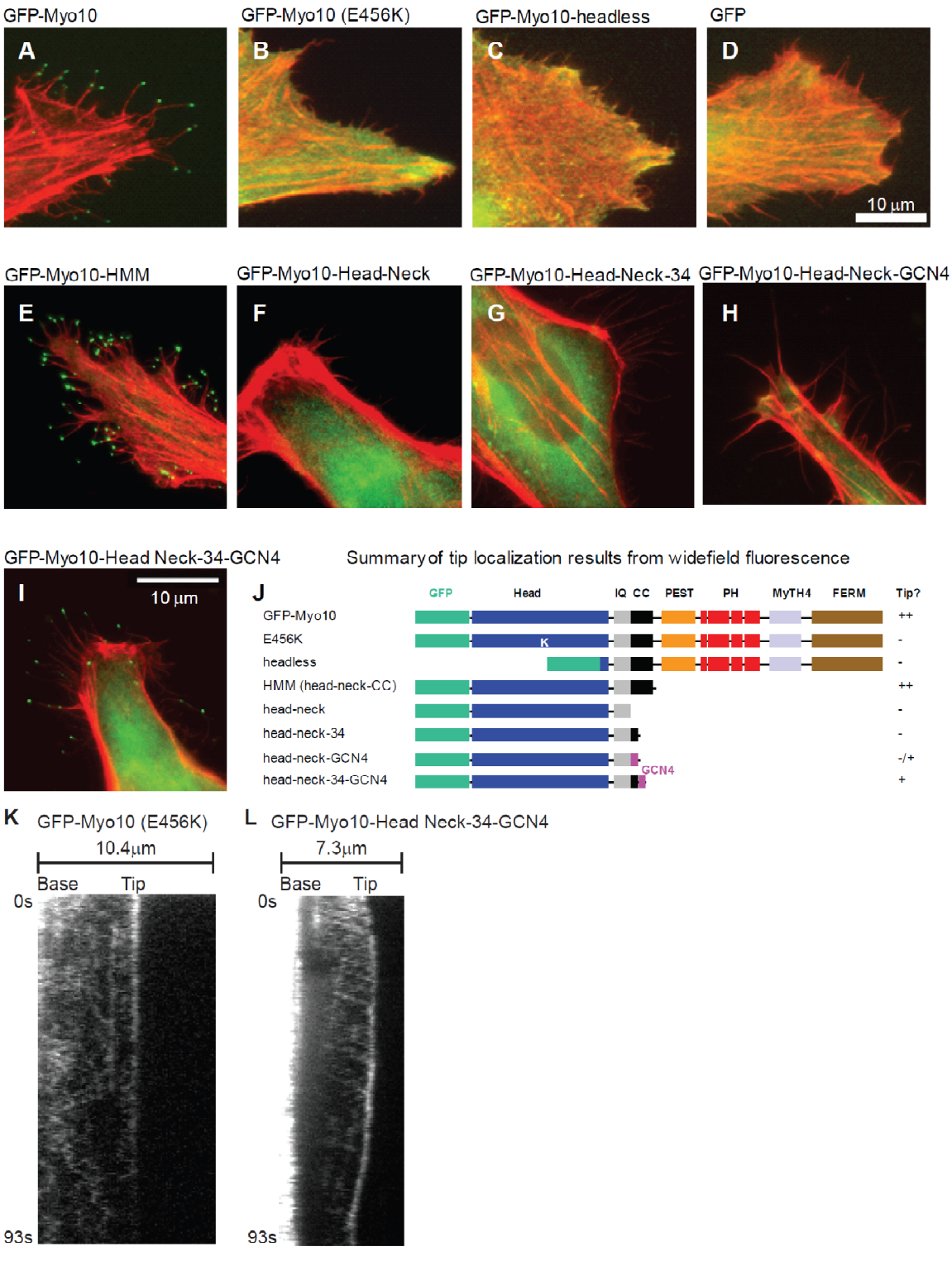
GFP-Myo10
A
GFP-Myo10 (E456K)
B
GFP-Myo10-headless
C
GFP
D
10 µm
GFP-Myo10-HMM
E
GFP-Myo10-Head-Neck
F
GFP-Myo10-Head-Neck-34
G
GFP-Myo10-Head-Neck-GCN4
H
GFP-Myo10-Head Neck-34-GCN4
I
10 µm
Summary of tip localization results from widefield fluorescence
J
GFP
Head
IQ
CC
PEST
PH
MyTH4
FERM
Tip?
GFP-Myo10
++
E456K
K
-
headless
-
HMM (head-neck-CC)
++
head-neck
-
head-neck-34
-
head-neck-GCN4
-/+
head-neck-34-GCN4
GCN4
+
K
GFP-Myo10 (E456K)
10.4µm
Base
Tip
0s
93s
L
GFP-Myo10-Head Neck-34-GCN4
7.3µm
Base
Tip
0s
93s

Figure 2.6. Ability of different Myo10 constructs to localize to filopodial tips and TIRF imaging of a motor domain point mutant and a forced dimer construct

(**A-I**) HeLa cells transfected overnight with the indicated GFP-tagged constructs (green) were replated ~12 hours on glass coverslips, fixed, and then stained with phalloidin (red). (**A-D**) The full-length, positive control GFP-Myo10 shows clear localization to the filopodial tip, whereas GFP-Myo10 E546K (a motor domain point mutant), as well as the negative controls (GFP-Myo10-headless and GFP alone) show little or no localization to the tip, demonstrating that Myo10 motor activity is necessary for strong tip localization. (**E-I**) Similar experiment showing that the GFP-Myo10-HMM positive control is clearly sufficient for localizing to filopodial tips, whereas the GFP-Myo10-head-neck, GFP-Myo10-head-neck-34, and the GFP-Myo10-head-neck-GCN4 forced dimer show little or no tip localization. The slightly longer GFP-Myo10-head-neck-34-GCN4 forced dimer is able to localize to the filopodial tip, although it also exhibits some diffuse labeling of the cell body. (**J**) Bar diagram summarizing the domain structure of different Myo10 constructs and their ability to localize to the filopodial tip. (**K**) Kymograph of a filopodium from a cell transfected with the motor domain point mutant (GFP-Myo10 E456K) and imaged by TIRF. The motor domain point mutant showed little localization to the filopodial tip relative to wild type GFP-Myo10 and did not generate clear tracks corresponding to rapid forward movements. (**L**) Kymograph of a filopodium from a cell transfected with the GFP-Myo10-head-neck-34-GCN4 forced dimer and imaged by TIRF. This construct generated occasional tracks corresponding to fast forward movements, indicating that a forced dimer is capable of rapid forward movements within filopodia.

dimerization of the head-neck region is sufficient for fast forward movement and tip localization.

To test whether the fast forward movements are dependent on actin, cells were treated with 1 μM latrunculin B to depolymerize actin filaments. As expected, this triggered the collapse of filopodia that were not attached to the substrate (not shown). Although latrunculin did not induce collapse of most substrate-attached filopodia, it did cause the loss or spreading of the bright puncta of GFP-Myo10 normally present at their tips (Figure 2.5C). Most importantly, fast forward movements of GFP-Myo10 were not detected after treatment with latrunculin B, indicating that the fast forward movements are indeed dependent on F-actin. Treatment of cells with 5 μM nocodazole did not block fast forward movements of GFP-Myo10 (data not shown).

Faint particles of GFP-Myo5a undergo similar movements

To test whether other myosins were capable of similar movements within filopodia, we imaged HeLa cells transfected with GFP-Myo1a (brush border myosin I), a monomeric myosin that is non-processive and localizes to microvilli (Tyska and Mooseker, 2002). TIRF showed that GFP-Myo1a yielded a diffuse localization along the filopodia with no obvious enrichment at the filopodial tip (Figure 2.7A). Importantly, GFP-Myo1a did not undergo detectable fast forward movements in filopodia, indicating that not all myosins are capable of rapid directed movements in filopodia. We also tested GFP-Myo5a (Wu et al., 2002), an intensively studied dimeric myosin that is processive and functions in organelle transport (Trybus, 2008) and filopodial dynamics (Wang et al.,

1996). Interestingly, GFP-Myo5a was enriched at the tips of filopodia and faint particles of GFP-Myo5a generated clear tracks corresponding to rapid forward movement (Figure 2.7B). However, the GFP-Myo5a particles moved at only ~251 +/- 121 nm/s (59 measurements from 22 filopodia), significantly (P=0.035) slower than the ~578 nm/s observed for GFP-Myo10. The velocity of the GFP-Myo5a particles is very similar to the 270-330 nm/s reported for individual molecules of a dimeric Myo5a construct moving on actin bundles *in vitro* (Nagy et al., 2008). It is therefore likely that the rapid and directed movements of GFP-Myo5a detected here correspond to the visualization of individual Myo5a molecules moving along the actin filaments of living cells. As with GFP-Myo10, faint particles of GFP-Myo5a sometimes moved slowly rearward at the retrograde flow rate of ~10-20 nm/s (Figure 2.7B). This observation provides direct evidence that Myo5a can indeed undergo retrograde flow, as recently hypothesized (Liu et al., 2006).

Conclusions

The TIRF experiments reported here reveal a novel form of long-range motility driven by myosin motors at or near the single-molecule level. The fast movements require Myo10 motor activity and actin filaments, but not the Myo10 tail. Together, these results strongly support the hypothesis that Myo10 molecules use their barbed-end motor activity to move forward along filopodial actin filaments (see model illustrated in Movie S5). The faint particles detected with TIRF exhibit a size, intensity range, and bleaching behavior consistent with imaging at the single-molecule level. It is not yet clear, however, whether these particles correspond to monomers, dimers, or small

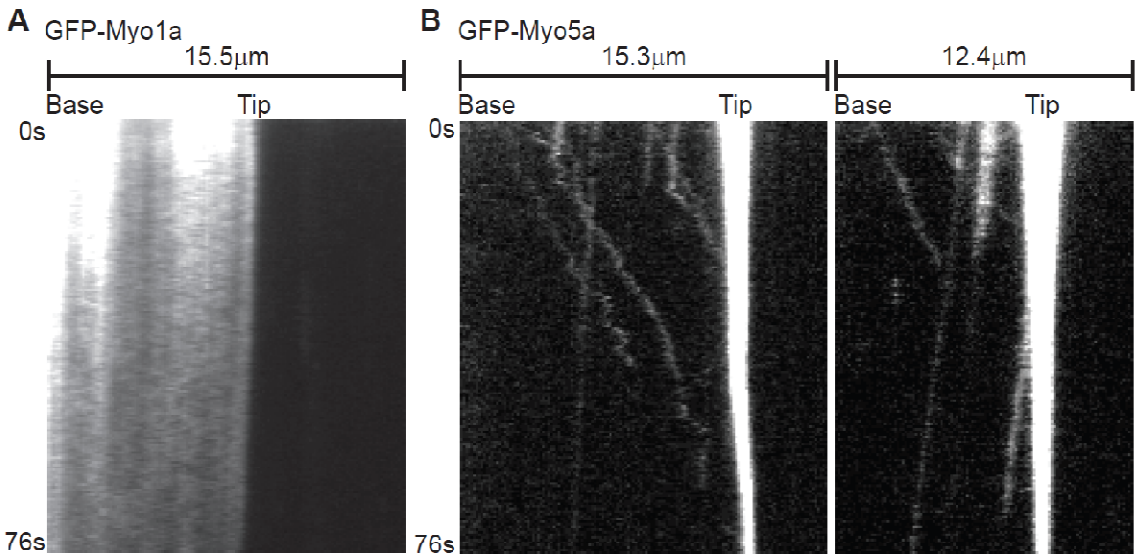

Figure 2.7. Particles of GFP-Myo5a also move forward and rearward in the filopodia of living cells

(**A**) Kymographs from TIRF imaging of GFP-Myo1a in filopodia. GFP-Myo1a did not localize to the tips of filopodia and no tracks corresponding to rapid forward movement were detected. (**B**) Kymographs from TIRF imaging of GFP-Myo5a in filopodia. Note that several faint particles of GFP-Myo5a moved rapidly towards the tip while others moved slowly rearward.

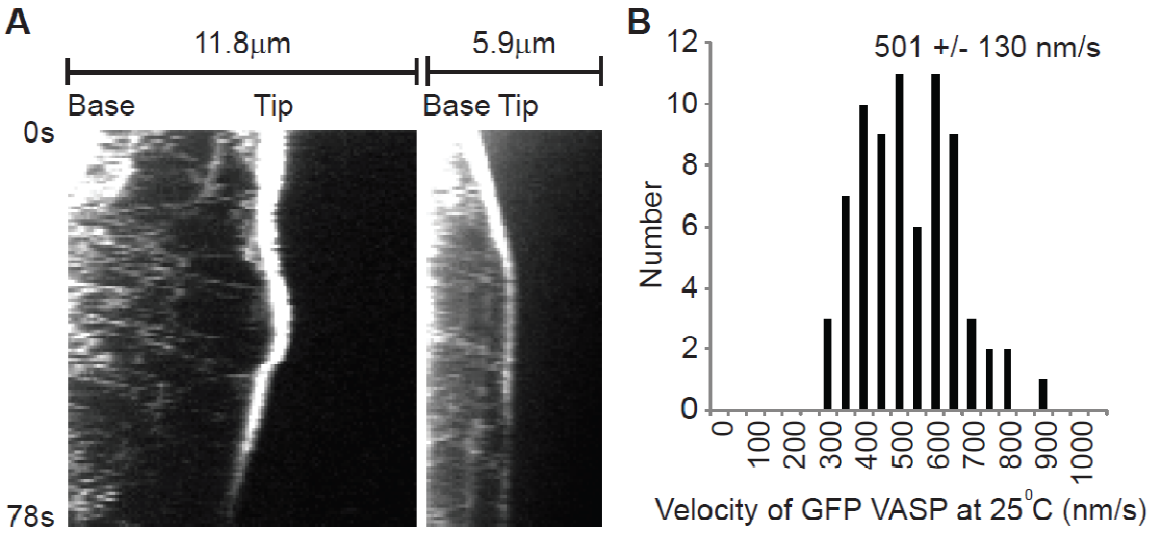

Figure 2.8. Faint particles of GFP-VASP move rapidly forward in filopodia at velocities similar to those of GFP-Myo10

(**A**) Kymographs of filopodia from HeLa cells transfected with GFP-VASP and imaged using standard TIRF imaging conditions. Note that GFP-VASP localizes to filopodial tips and generates faint tracks corresponding to rapid forward movement. (**B**) Velocity histogram for fast forward movements of GFP-VASP particles.

oligomers of Myo10. Several factors contribute to this uncertainty, including the relatively high and variable background fluorescence present in living cells, variable levels of protein expression, the non-ideal behavior of GFP as a fluorophore, and variations in the Z-axis position of the filopodium or molecules within it. For example, even a 0.1 um difference in the Z-axis position (the approximate thickness of a filopodium) will result in a ~2-fold change in the intensity of the TIRF field. It should also be noted that although we can clearly detect the movements of some particles, we cannot guarantee unambiguous detection of every GFP-Myo10 molecule in a filopodium. Despite these limits, the combination of TIRF and GFP-tagging used here provides a powerful strategy for imaging the movements of motor proteins and their cargos at or near the single-molecule level in living cells.

In addition to exhibiting a novel form of rapid, long-range motility in filopodia, Myo10 also has potent filopodia-promoting activity. Our previous work indicates that Myo10's ability to induce numerous filopodia requires (1) elements within the Myo10 tail and (2) the ability to localize to filopodial tips (Bohil et al., 2006). Since we now find that only Myo10 constructs capable of moving rapidly forward in filopodia are able to localize to filopodial tips, the novel form of motility reported here is likely to underlie both tip localization and filopodia promotion. Although the precise mechanism(s) by which My10 promotes filopodia are not yet clear, it could act by initiating filopodia, by transporting cargos that facilitate filopodia formation, by functioning as part of a mobile tip complex, or by some combination of these or other mechanisms (Bohil et al., 2006; Sousa and Cheney, 2005; Tokuo et al., 2007).

As a motor that moves rapidly along filopodia, Myo10 clearly transports itself to the filopodial tip, but it may also be responsible for the transport of other specific molecular cargos, such as VASP(Tokuo and Ikebe, 2004). Indeed, preliminary experiments indicate that faint particles of GFP-VASP exhibit fast, forward movements in filopodia very similar to those of Myo10 (Figure 2.8). A major goal for the future will be to test for cotransport at the single-molecule level and to determine whether Myo10 is required for transport of this and other cargos. It will also be interesting to determine if Myo3a or Myo15a, myosins that localize to the tips of stereocilia and are necessary for hearing, undergo similar forms of movement (Belyantseva et al., 2005; Liu et al., 2006; Schneider et al., 2006). In addition to revealing a novel form of motility, this work also suggests that motor proteins may power many as yet undetected movements at the single-molecule level.

Materials and Methods

Constructs. Bovine GFP-Myo10 (aa 1-2052), GFP-Myo10-HMM (aa 1-947), and GFP-Myo10-head-neck (aa 1-811) in pEGFP-C2 have been described previously (Berg and Cheney, 2002). The GFP-Myo10 E456K motor domain point mutant (GAG>AAG, nt 1588-1590) was generated by PCR in pEGFP-C2 and corresponds to a weak actin-binding mutation in other myosins(Friedman et al., 1998). The GFP-Myo10-head–neck-GCN4 forced dimer was generated by fusing the 29 aa leucine zipper (VKQLEDKVEELASKNYHLENEVARLKKLV) from yeast GCN4 to aa 811 of the bovine Myo10-head-neck construct and cloning this into the BglII-HindIII sites of pEGFP-C2. The GFP-Myo10-head-neck-34 construct consists of aa 1-845 of bovine

Myo10 inserted into the BglII-HindIII sites pEGFP-C2. The GFP-Myo10-head-neck-34-GCN4 construct was identical except that the GCN4 leucine zipper sequence was added after aa 845. Myo10 constructs were verified by sequencing and their numbering is based on GenBank sequence NM_174394. Mouse GFP-Myo1a in pEGFP-C (Tyska and Mooseker, 2002) was a generous gift from Dr. Matthew Tyska, mouse brain GFP-Myo5a in pEGFP-C1 ("BR MV")(Wu et al., 2002) was a generous gift of Dr. John Hammer, human GFP-VASP in pEGFP-N1 was a generous gift from Dr. Frank Gertler, and pEGFP-C2 was used as a GFP control.

Cells. HeLa cells were transfected with Polyfect (Qiagen) unless indicated otherwise. To obtain the relatively low levels of expression required to facilitate single-molecule imaging, HeLa cells were generally transfected for no more than 6-12 hours. Cells were replated onto #1.5 glass coverslips that had been precoated with fibronectin to facilitate formation of substrate-attached filopodia. Coverslips were precoated by incubating acid-washed coverslips for 20 minutes in 10 µg/ml fibronectin in PBS and then washed at least 3x in PBS over 10 minutes prior to plating. To minimize background from cellular debris, cells were usually plated onto coverslips at <10% confluence, with best results obtained with less than one cell per camera field. Cells were allowed to attach to the coverslip for 1-2 hours and the coverslip was mounted in a Rose chamber with a 3 mm spacer and a #1.5 coverslip for the roof. The chamber was completely filled with Optimem (Gibco). Tet-off HeLa cells (Clontech) that "stably" express GFP-Myo10 were generated as per the manufacturer's instructions. These cells were withdrawn from doxycycline for 1 day to induce expression of GFP-Myo10 and then plated onto glass

coverslips and imaged as described above. Only a subset cells expressed detectable GFP-Myo10 following doxycycline withdrawal.

Imaging. Objective type TIRF imaging was performed with a Nikon TE-2000U inverted microscope equipped with a Nikon TIRF-II illuminator with 18 mm field of view, a 60x 1.45 NA lens, and a 100 W Hg lamp. TIRF illumination was provided by a 300 mW argon laser and a AOTF was used for rapid wavelength selection and shuttering. For single-molecule experiments, the laser power at 488 nm was adjusted to approximately 40 mW, measured upon exit from the fiber optic cable leading to the TIRF illuminator. The calculated penetration depth for the TIRF field under our standard conditions is ~160 nm. During TIRF imaging, all neutral density filters were removed from the beam path in the TIRF-II illuminator. As noted, in some experiments a Nikon single-molecule TIRF illuminator with an 11 mm field of view was used in place of the TIRF II illuminator. A Chroma #41001 filter cube was used for GFP imaging and images were captured on an ORCA-ER cooled CCD camera (Hamamatsu). Standard camera settings were low light mode, zero gain, and no binning, with a pixel size of 107 nm. 200 ms exposures were typically collected at 2-3 frames/s for 30-90 s and the 488 nm laser line was active only during exposures. Using a 1.45 NA lens with 488 nm light at 63° incidence, the calculated penetration depth of the TIRF field (distance to decay to 1/e of intensity at coverslip surface) is ~158 nm. Experiments were performed at 25° C unless indicated otherwise. To avoid pre-bleaching cells prior to a time-lapse series, we generally focused on a cell, and adjusted the laser angle to establish TIRF, shuttered the laser, moved the stage to a different cell in an adjacent field that had not been illuminated,

checked focus with DIC, and then activated the laser and acquired the time-lapse. When the performance of the TIRF system was compared to conventional widefield fluorescence with a 100 W mercury lamp by imaging the tips of substrate-attached filopodia, TIRF images acquired under identical exposure conditions were approximately an order of magnitude brighter and exhibited greatly decreased background. Metamorph 7.5 software was used to control the microscope, acquire images, adjust contrast, and scale images. Adobe Photoshop and Illustrator were used to prepare figures.

Kymotracker and data analysis. Imaging data was analyzed using custom software written in Python. The user draws a line through a filopodium and this software generates a kymograph. The user then traces the particle tracks on the kymograph. This position information is used to seed a center-weighted spot search. The program then performs a fixed-radius Gaussian fit which determines the intensity, background, and subpixel location of the spot in each image. To achieve a more accurate background measurement, the Gaussian fit algorithm ignores nearby pixels which deviate from the Gaussian model by a predefined amount. Kymotracker will attempt to fit a Gaussian even for time points in which no particles are present, finding the brightest area in the naturally variable background and thus reporting a slight positive intensity instead of zero after a spot has bleached. The values reported after bleaching are a good indication of the level of variation in background pixel intensities and are easily distinguished from the typical intensities of bona fide spots. Kymotracker outputs this data as a file that can be opened in Microsoft Excel for graphing and further analysis. For each track, Kymotracker also captures an image of the spot at each time point. The Kymotracker software is

available upon request. Particle velocities were calculated from the slopes of kymograph tracks. Error bars indicate standard deviations. Statistical significance was calculated using a 2-tailed t-test for unequal sample size and unequal variance.

Supplemental Movie Legends

Movie S1. TIRF Microscopy of Single GFP Molecules Adsorbed on a Coverslip.

Pure GFP (Clontech) was diluted with TBS, adsorbed to #1.5 glass coverslips, and washed several times with TBS and then imaged using TIRF. As expected for single-molecule imaging, several faint, diffraction-limited spots are present at the beginning of the time-lapse and exhibit stepwise bleaching. Several spots also "blink" on and off, a behavior that is a hallmark of single molecule imaging with GFP. This time-lapse was acquired using the standard TIRF imaging conditions of 200 ms exposures, 2-3 frames/s, and 107 nm pixels. Time stamps indicate minutes:seconds and scale bars indicate 5 um.

Movie S2. TIRF Microscopy of GFP-Myo10 in HeLa Cell Filopodia. This time-lapse was acquired under the same imaging conditions as Movie 1 and shows bright puncta of GFP-Myo10 at the tips of the numerous substrate-attached filopodia/retraction fibers. In addition to these bright puncta, large numbers of extremely faint particles of GFP-Myo10 can be detected moving within the shafts of the filopodia. GFP-Myo10 can also be detected in the thicker part of the cell at the bases of the filopodia, but much of this region of the cell is saturated under the imaging and scaling conditions used here.

Movie S3. TIRF Microscopy Reveals Fast Forward Movements of Faint Particles of GFP-Myo10 in a Filopodium. This time-lapse movie illustrates the rapid and directed movements of several faint particles of GFP-Myo10 towards the tip of a filopodium. This is the same filopodium illustrated in Figure 2.1A-B and was acquired under the standard TIRF imaging conditions.

Movie S4. TIRF Microscopy Illustrating both Fast Forward and Slow Rearward Movements of GFP-Myo10. This time-lapse shows numerous faint particles of GFP-Myo10 moving in a rapid and directed manner to the tip of the filopodium. These images were acquired under the same conditions as above except that a single-molecule TIRF illuminator was used. A kymograph from this time-lapse is shown in Figure 2.2B.

Movie S5. Model of Intrafilopodial Motility of Myo10. This video schematically illustrates a filopodium containing a single actin filament with actin monomers (red) polymerizing at the barbed end and undergoing retrograde flow at 10-20 nm/s. A Myo10 molecule, illustrated here as a dimer, uses its motor activity to move forward on filopodial actin in a rapid and directed fashion at ~600 nm/s. A large tip complex that includes tens or hundreds of Myo10 molecules is present at the filopodial tip. Rearward movement of Myo10 results from tight binding to actin filaments undergoing retrograde flow.

Acknowledgements

DTJ was supported by a Porter Fellowship from the APS and a UNC Sequoyah Dissertation Fellowship. TY was supported by the Leukemia and Lymphoma Society and OAQ was supported by a UNC SPIRE postdoctoral fellowship from NIH/GM00678. This research was supported by NIH/NIDCD grant RO1 DC03299 to REC and by NIH/NHLBI grant P01 HL080166.

Chapter 3: Investigations of the role of Myo10 in a filopodial tip complex

Summary

How do cells sense and interact with their environment? Many cells extend fingerlike protrusions, called filopodia, that have been hypothesized to function as sensors. For example, macrophage filopodia appear to scan their surroundings, adhere to pathogens, and reel them back towards the cell body. The roles of filopodia in processes such as pathogen capture and cell migration are mostly correlative, however, since there is not yet a way to specifically inhibit filopodia in vivo. Certain capabilities of filopodia, such as their adhesion to substrates, seem indisputable despite a poor understanding of the mechanism of filopodial adhesion. One candidate for directly linking the membrane receptors to the actin cytoskeleton is the molecular motor, myosin-X, which is the best known marker for filopodial tips. Additionally, myosin-X may deliver adhesion machinery to the tips of filopodia, perhaps serving double-duty as an intrafilopodial transporter and anchor. Here, I describe preliminary experiments intended to investigate the role of Myo10 in filopodial adhesion. An accurate model of the molecular underpinnings of filopodia is a crucial step towards finally establishing their functions in vivo.

Introduction

Filopodia are cellular protrusions resembling antennae in their form and presumed function. There is compelling evidence indicating that filopodia are able to detect chemical and physical environmental signals, form attachments to substrates and other cells, and use those attachments to apply force (Faix and Rottner, 2006; Mattila and Lappalainen, 2008). Filopodia are therefore thought to function in several biological processes, including axon guidance and the capture of pathogens by immune cells (Koleske, 2003; Kress et al., 2007).

The filopodial tip is thought to be the "business end" of the structure, and unpublished data from our lab reveals the presence of a dense complex at the filopodial tip (Figure 3.1). This filopodial tip complex is likely to include proteins reported to localize to tips, including the molecular motor, myosin-X (Myo10); the actin filament anti-capping protein, VASP; and the extracellular matrix receptor, integrin (Berg and Cheney, 2002; Tokuo and Ikebe, 2004; Zhang et al., 2004). The composition of the tip complex is largely unknown, but during early spreading, initial attachments are mediated by filopodia that contain known focal adhesion proteins, including integrin and talin (Partridge and Marcantonio, 2006).

Focal adhesions are protein complexes that span the cell membrane and anchor the cell to the extracellular matrix (ECM) (Dubash et al., 2009; Zamir and Geiger, 2001). These adhesions generally rely on the integral membrane protein, integrin, to bind to ECM proteins. Integrins are heterodimers with many different α and β subunits, which when paired in different combinations can bind specifically to different ECM proteins. For example, the $\alpha5\beta1$-integrin heterodimer binds specifically to fibronectin while the

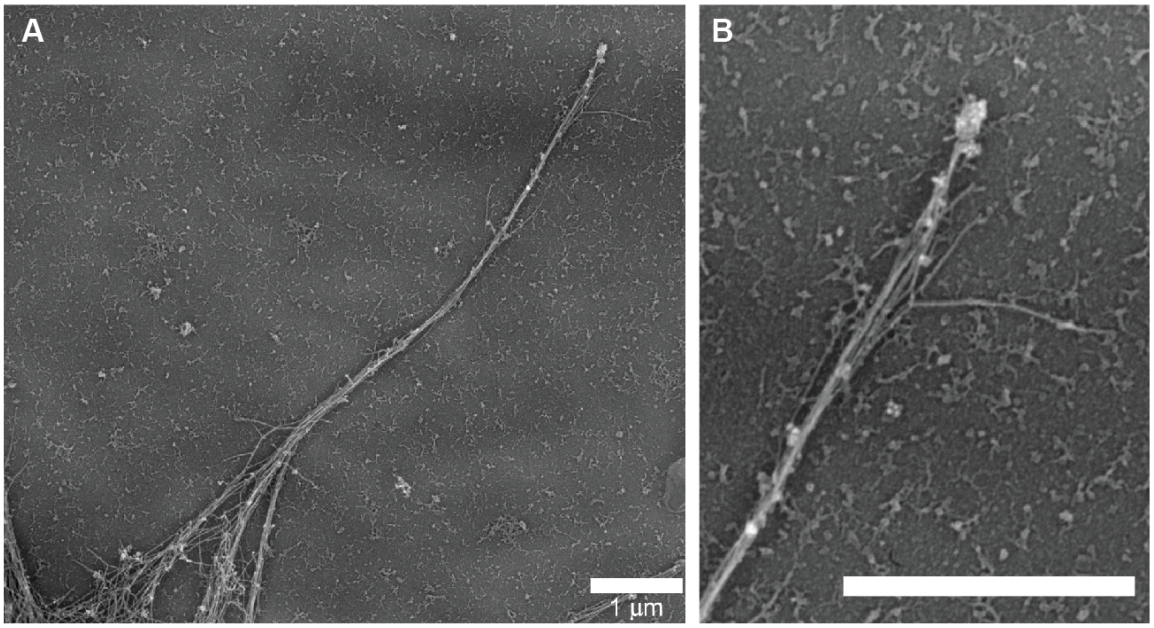

Figure 3.1. Platinum replica electron micrograph of an individual filopodium

(**A**) Filopodium from a cell fixed using the methods described by the Borisy group (Svitkina et al., 2003), removing the plasma membrane while preserving the structure of the actin cytoskeleton. In this image, the cell body is towards the lower left and the filopodium extends towards the upper-right. (**B**) Higher-magnification view of filopodial tip from A. Note the presence of a large, amorphous group of proteins at the filopodial tip. Scale bars represent 1 um. Image provided by Omar Quintero.

αvβ3 heterodimer binds to vitronectin (Hermann et al., 1999; Morgan et al., 2009). The intracellular portion of integrin binds to adapter proteins like talin, which are thought to form the link between the focal adhesion and the actin cytoskeleton (Burridge and Mangeat, 1984; Horwitz et al., 1986; Samuelsson et al., 1993). Myo10 is not found in focal adhesions, but it has been reported to interact with the cytoplasmic domains of β1, β3, and β5 integrin subunits via a FERM domain in its tail (Zhang et al., 2004). Since Myo10 can also bind to actin via its motor domain, it is a strong candidate for acting as a structural link between integrins and filopodial actin.

While a daunting number of proteins are known to associate with focal adhesions, integrin, talin, and vinculin are among those known to be essential. Intriguingly, both talin and vinculin appear to contribute to filopodial stability (Sydor et al., 1996). When vinculin is inactivated by chromophore assisted laser inactivation (CALI) in the neuronal growth cone, filopodia in the affected region reportedly buckle more often than usual. When talin is inactivated, the filopodia tend to stall, halting extension and retraction. The researchers who performed these experiments concluded that talin regulates filopodial extension while vinculin bundles filopodial actin. An alternative explanation is that they were instead responsible for forming adhesions that are required for continued extension of filopodia along the plane of the growth cone.

How might adhesion proteins localize to the tips of filopodia? Computational models of filopodia suggest that diffusion alone is insufficient to allow for the accumulation of "consumed" proteins at filopodial tips, which can sometimes extend several microns from the cell body (Zhuravlev et al., 2010). Consumed proteins refer to proteins like actin monomers, which are constantly added to the barbed ends of filaments

at the tip, but may also include adhesion components that are continuously deposited as a filopodium extends. Myo10 has been proposed to supplement diffusion by transporting proteins specifically towards filopodial tips, where it accumulates. Myo10's reputation as a motor that moves along filopodial actin is certainly long-standing and well established (Berg and Cheney, 2002).

Myo10 undergoes two modes of intrafilopodial motility: 1) "faint particles" of Myo10 frequently move in a directed fashion from the cell body towards filopodial tips at ~600 nm/s, and 2) "bright puncta" of Myo10, which are often observed undergoing retrograde flow in filopodia, sometimes migrate forward at ~80 nm/s (Kerber et al., 2009). VASP has been reported to undergo cotransport with the bright puncta of Myo10 and has also been shown to exhibit the frequent, fast movements indicative of the faint particles of Myo10 (Tokuo and Ikebe, 2004). Similar cotransport of integrins has not been reported, but beads coated with anti-integrin antibodies have been shown to migrate along filopodia at ~600 nm/s (Grabham et al., 2000). Furthermore, overexpression of Myo10 causes integrins to relocate to filopodial tips (Zhang et al., 2004). These data suggest two possible roles for Myo10 in filopodia: 1) as a transporter of other proteins, and 2) as a direct link between integrins and the actin cytoskeleton (Nambiar et al., 2010).

Results

Investigating the role of Myo10 in integrin transport

Integrin, an essential component of focal adhesions, localizes to filopodia and binds to the FERM domain of Myo10, and integrin-bound beads move along filopodia at

velocities similar to Myo10 movement rates. Although these pieces of the puzzle seem to form an obvious picture, evidence of direct transport of integrins by Myo10 has remained elusive. The ideal method to test whether Myo10 is required for transport of cargos like integrin is to knock out Myo10. If, in the complete absence of Myo10, integrins continue to exhibit intrafilopodial motility and localization to filopodial tips, then we could conclude that Myo10 is not required for their transport. If re-expression of full length Myo10 rescues integrin transport, while a Myo10 construct lacking the FERM domain does not rescue transport, then we could conclude that Myo10 is sufficient, but binding to integrins is required. Unfortunately, Myo10 knockout cells do not exist.

Knocking down Myo10 expression is also not an ideal method for determining its necessity for cargo transport. Myo10 plays an important, if poorly understood, role in filopodium formation. Knocking down Myo10 using siRNA has the confounding effect of reducing filopodia number (Bohil et al., 2006). Under these circumstances, it is possible that the few remaining filopodia persist because they retain an adequate amount of Myo10. Instead of having filopodia that contain less Myo10, there may be fewer filopodia with normal amounts of Myo10. It would then be misleading to study the effects of Myo10 knockdown in these remaining filopodia because they may still contain Myo10. Indeed, in HeLa cells in which Myo10 expression is stably knocked down, VASP continues to localize to the remaining filopodia (Figure 3.2). This suggests that the remaining Myo10 is sufficient for VASP localization or that VASP localizes in a Myo10-independent manner.

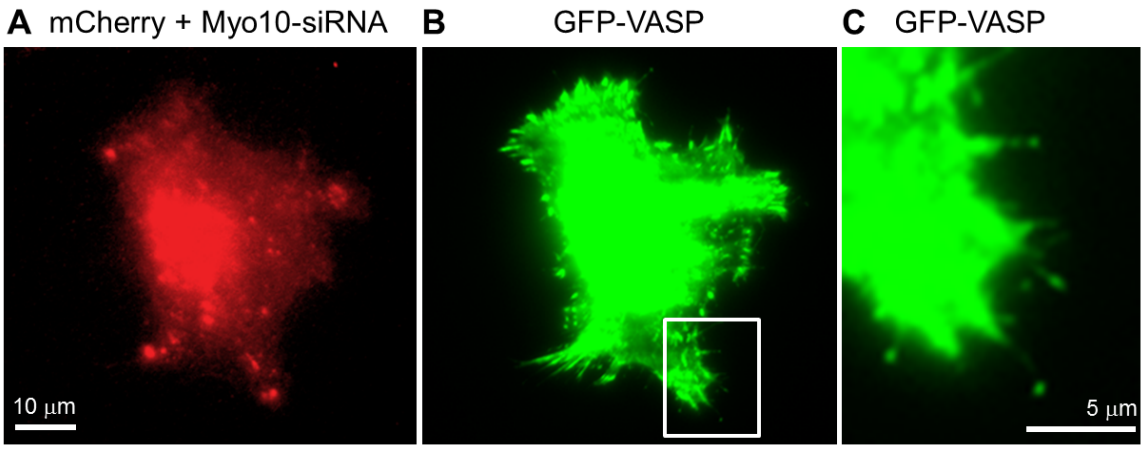

Figure 3.2. VASP localizes to filopodia in Myo10 knockdown cells

(A) HeLa cell stably expressing mCherry and siRNA against Myo10. (**B**) TIRF image of cell from (**A**) showing GFP-VASP localization to focal adhesions. (**C**) Higher magnification view of box from (**B**) showing GFP-VASP localization to filopodia.

An alternative method to demonstrate coordinate movement of Myo10 and integrins in filopodia is to image tagged versions of each molecule and determine whether they move in lock-step. As mentioned previously, Myo10 exists in two distinct populations in filopodia: bright puncta and faint particles. Each population of Myo10 exhibits a distinct forward velocity in filopodia, but both undergo retrograde flow at ~15 nm/s. The bright puncta of Myo10 appear to be associated with a slight bulge in the shaft of the filopodium. These bulges may represent large protein complexes or simply regions where the filopodium is engorged with cytoplasm or membrane. Colocalization of other proteins to these bulges might therefore be interpreted as nonspecific. The faint particles of Myo10 likely represent single molecules or dimers, and colocalization of proteins at the single-molecule level would be quite convincing. Unfortunately, single-molecule tracking of Myo10 in living cells has only recently been accomplished and our preliminary attempts at tracking even Myo10 labeled with fluorophores other than GFP have failed. At this time, we are unable to simultaneously track two molecules labeled with different fluorophores with single-molecule sensitivity in live cells.

Single-molecule tracking of integrins

If integrins do undergo cotransport with Myo10, one would expect to detect integrins exhibiting the same frequent, fast forward movement that we detect when we image Myo10 or VASP with our highly sensitive total internal reflection fluorescence (TIRF) microscopy system. To test for Myo10-like movements of integrins, we imaged HeLa cells overexpressing GFP-labeled β1 or β5 integrins, with or without simultaneous overexpression of their complementary alpha integrins (α5 and αv, respectively), and

also with or without expression of mCherry-Myo10. In cells expressing either GFP-β1 or -β5 alone, we observed diffuse localization of the integrins to the plasma membrane and accumulation in structures that resembled ER, with very little enrichment in focal adhesions or filopodia. Co-expression of the complementary α-integrin resulted in increased localization to focal adhesions. Localization to filopodia under these conditions, however, remained minimal and we were unable to detect single-molecule movements. It is possible the overexpression of integrins overwhelms the supply of endogenous Myo10. To relieve this potential traffic jam, we also overexpressed mCherry-Myo10 in these cells, leading to an increase in filopodia and enhanced integrin localization to filopodia. Enrichment at filopodial tips, however, was not observed under any of these conditions. Instead, integrins localized uniformly along filopodial shafts.

Since these results were not consistent with reported endogenous integrin localization, we attempted to optimize our imaging conditions by systematically varying several experimental parameters. To test whether integrin localization was dependent on the substrate, cells were plated on fibronectin, vitronectin, or uncoated glass. To test whether localization was dependent on the length of time that the cells were given to spread, we imaged at time points ranging from immediately after plating to 7 days after plating. Likewise, expression time for each construct was varied from 6 hours to 14 days to tailor the expression level for imaging of single-molecules. Unfortunately, allowing the cells to spread for more than 16 hours tended to increase background fluorescence of the substrate, making single-molecule tracking impossible. Ultimately, we found that the best imaging conditions were achieved in cells that were allowed to spread on fibronectin for 1 hour, expressed both GFP-β and GFP-α integrins for 7 days, and expressed

mCherry-Myo10 for 6 hours. Even under these optimized conditions, although integrins did appear enriched at the cell periphery and in filopodia, they were not enriched at filopodial tips. Although we detected a few integrin particles that exhibited fast, forward movement, these events were brief and rare (Figure 3.3). These single integrin molecules moved forward at roughly 350-450 nm/s compared to the ~600 nm/s that we reported for Myo10 and run lengths were typically only 1-2 um, compared with Myo10's ability to travel 10 um in a persistent fashion.

Although previous single-molecule imaging experiments were able to reveal populations of Myo10 and VASP that undergo frequent, fast, forward intrafilopodial movement, similar methods were unable to detect an analogous population of integrins. Does this mean that Myo10 does not transport integrins in filopodia? It is still possible that the population of Myo10 responsible for integrin transport is the previously-observed, slower moving, large clusters of Myo10. Indeed, clusters of integrins have been observed undergoing cotransport with these Myo10 clusters within filopodia (unpublished data from Melinda Divito). It is also possible that Myo10 interacts with integrins very weakly, resulting in short-lived interactions that drag integrins short distances forward and bias their localization only slightly toward filopodial tips. Competition with other integrin binding partners, like talin, could also limit the binding time between Myo10 and integrin and would provide the cell with a way to balance integrin forward transport with deposition along filopodial shafts. A definitive conclusion to the story of Myo10 and integrin transport in filopodia may require the development of Myo10 knockouts or an imaging system capable of tracking single-molecules in two colors.

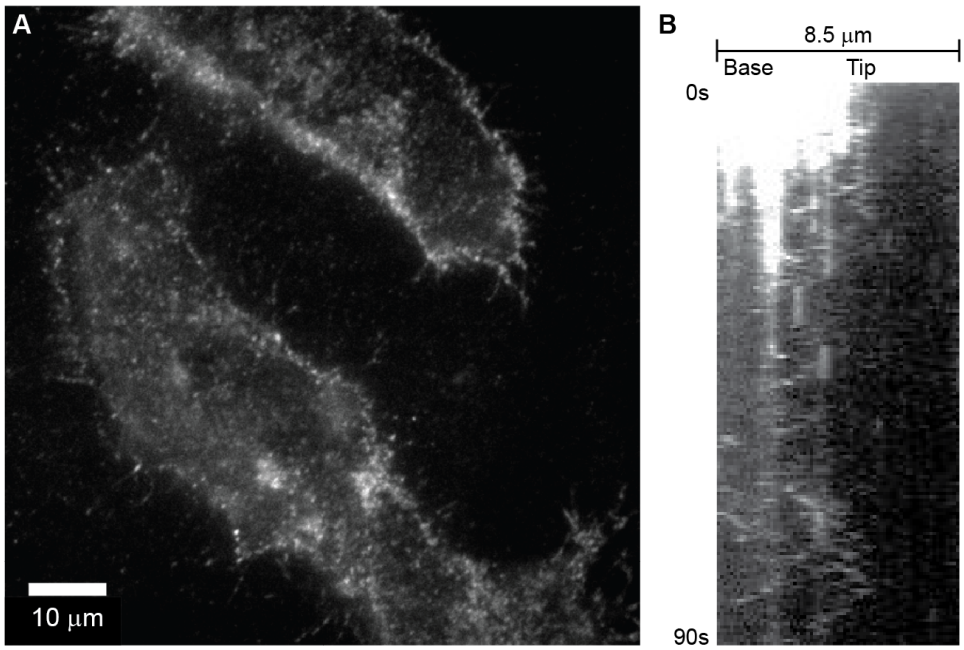

Figure 3.3. Single-molecule imaging of integrins reveals occasional forward movements

(**A**) HeLa cells transfected with GFP-α5 and GFP-β1 for five days and mCherry-Myo10 for three days. Cells imaged using single-molecule TIRF after given one hour to spread. Spots seen in this image from the GFP channel of a timelapse video exhibited characteristic single-molecule intensities and blinking. (**B**) Example kymograph of a filopodium from A. Note several vertical tracks, representing stationary particles. Velocities of forward moving particles range from 350 – 450 nm/s.

Investigating the role of Myo10 in linking integrins and F-actin

CALI of Myo10 at tips

Myo10's potential role as a cargo transporter does not exclude the possibility that it functions as a direct link between integrins and filopodial actin in nascent adhesions (Nambiar et al., 2010). It is hypothesized that these nascent contacts are eventually converted into mature adhesions as focal adhesion proteins like talin and vinculin are recruited to the site (Partridge and Marcantonio, 2006). We hypothesize that the initial contact between a filopodial tip and the extracellular matrix is secured to the cell's actin cytoskeleton by Myo10 (Zhang et al., 2004).

If cells were like ships anchored at sea, filopodia would be the ropes leading down to the anchors, which would be analogous to the integrins of a focal adhesion. Proteins like Myo10 and talin would serve as chain links to connect the anchor to the filopodial rope. Damage one of the links, and the rope may recoil back towards the ship. How can we instantaneously inactivate a putative link in the focal adhesion chain? One promising method involves the use of a laser to excite free-radical-emitting dyes that can be linked to proteins of interest. Initial versions of this method, called chromophore-assisted laser inactivation (CALI), have already implicated talin and vinculin in filopodial stability (Sydor et al., 1996). CALI causes chromophores to generate short-lived reactive oxygen species (ROS) that damage proteins within an effective radius of ~15 angstroms, causing an acute and specific inactivation of the tagged proteins excited by the laser (Jacobson et al., 2008; Liao et al., 1994). Although CALI originally exploited the ROS-producing power of chromophores like malachite green, more recent experiments

demonstrate that CALI can be achieved with the genetically-encoded tag, GFP (Vitriol et al., 2007).

To determine whether CALI could be used to test Myo10's ability to link filopodial actin to nascent adhesions, we performed preliminary experiments with CALI in collaboration with the lab of Dr. Ken Jacobson, UNC Chapel Hill. For these experiments, we used HeLa cells in which Myo10 expression is stably knocked down and GFP-Myo10 is overexpressed. If Myo10 functions as a structural component of the filopodial adhesion, inactivation would cause either detachment of the filopodium from the substrate, or detachment and subsequent retrograde flow of the phase-dense tip spot within the filopodium. Using a 400 mW, 488 nm laser line tuned to 2.5 um in the sample plane, we were able to CALI the Myo10 tip spots of several filopodia per cell. We then used brightfield imaging to detect detachment events immediately after CALI. In almost all cases, no noticeable effect was detected after CALI. On two occasions, we detected retrograde flow of the phase dense tip spot after CALI, although these events are not uncommon in normal cells (Figure 3.4).

Is Myo10 involved in linking integrins to actin in filopodial adhesions? A statistical comparison of CALI-induced detachment in GFP-Myo10 cells compared to GFP-GPI or GFP-alone cells may be required to detect a potentially subtle effect. It is also possible that we did not successfully inactivate GFP-Myo10 and that the use of a better ROS-generating chromophore will be required. Ideally, the use of Myo10 knockout cells should be used in future experiments to eliminate the possibility that endogenous Myo10, which should be unaffected by CALI, is sufficient to maintain adhesion. Filopodial tip spots remain an ideal environment for performing CALI, due to

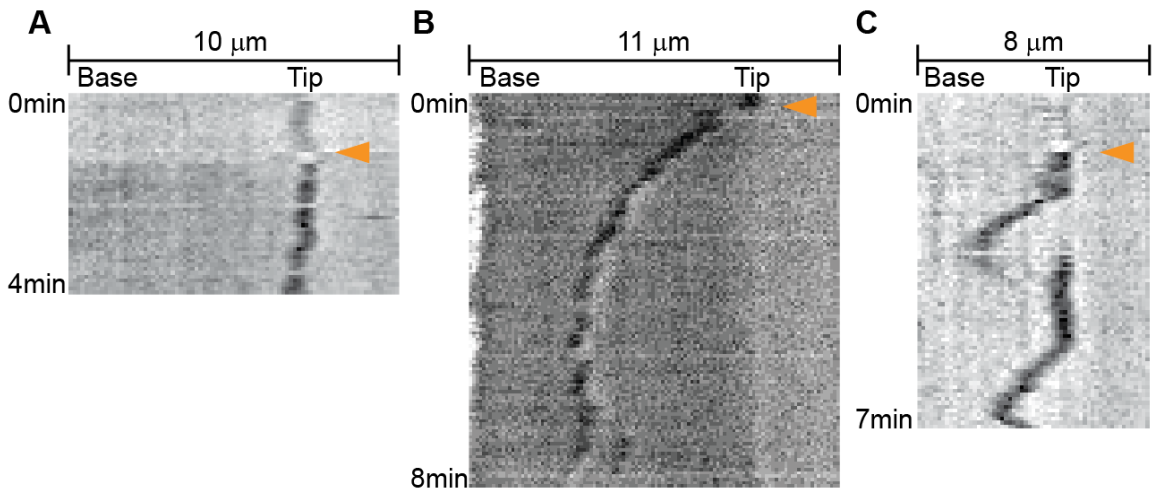

Figure 3.4. CALI of GFP-Myo10 tip spots

Example kymographs of filopodia from HeLa cells in which endogenous Myo10 is knocked down with siRNA and GFP-Myo10 is overexpressed. CALI is performed at the time point indicated by the orange arrows. Timelapse videos were acquired using brightfield. Dark tracks indicate the location of the tip bulge along the filopodium. (A) is representative of most observations; CALI has no obvious effect on the filopodium. (B-C) represent occasions when the tip bulge exhibited retraction immediately after CALI. Note that in these instances, the filopodium did not detach from the substrate; the tip bulge retracted within the filopodium. In (C), the tip bulge moves back to the tip after ~3 minutes and then undergoes a second rearward movement that was not instigated by CALI.

their distance from the cell body and their proximity to the coverslip. Unfortunately, CALI is an unlikely tool to study intrafilopodial transport since the powerful CALI laser pulse also instantaneously bleaches nearby fluorophores, making the tracking of fluorescent particles impossible. Moreover, the use of CALI is limited to the study of relatively immobile filopodia, due to the gap in time between positioning and firing the laser. We made several attempts to inactivate the tips of dynamic filopodia, but were unsuccessful in hitting these fast-moving, 100 nm structures with the slowly manipulated 2.5 um laser spot.

Use of optical tweezers to form nascent filopodial adhesions

Since CALI was limited to the study of stably-attached filopodia, the adhesions observed may not have been particularly nascent. We attempted to induce new filopodial adhesions by guiding glass or polystyrene beads into the filopodia of live HeLa cells. The advantages to this approach include the potential to measure the piconewton-scale forces that individual filopodia apply to the beads without disturbing the rest of the cell. The beads can also be coated with extracellular matrix proteins, such as fibronectin, to test for the involvement of integrin-specific attachments.

In our preliminary experiments, we were able to successfully "catch" filopodial tips in GFP-Myo10-expressing cells with optically trapped beads made of either glass or polystyrene and either coated with fibronectin or uncoated. The attached filopodia were then manipulated by maneuvering the trapped bead (Figure 3.5). We found that filopodia could be stretched past the initial site of the filopodial tip, marked by the Myo10 tip spot. Surprisingly, in trial experiments the Myo10 tip spot did not always follow the point of

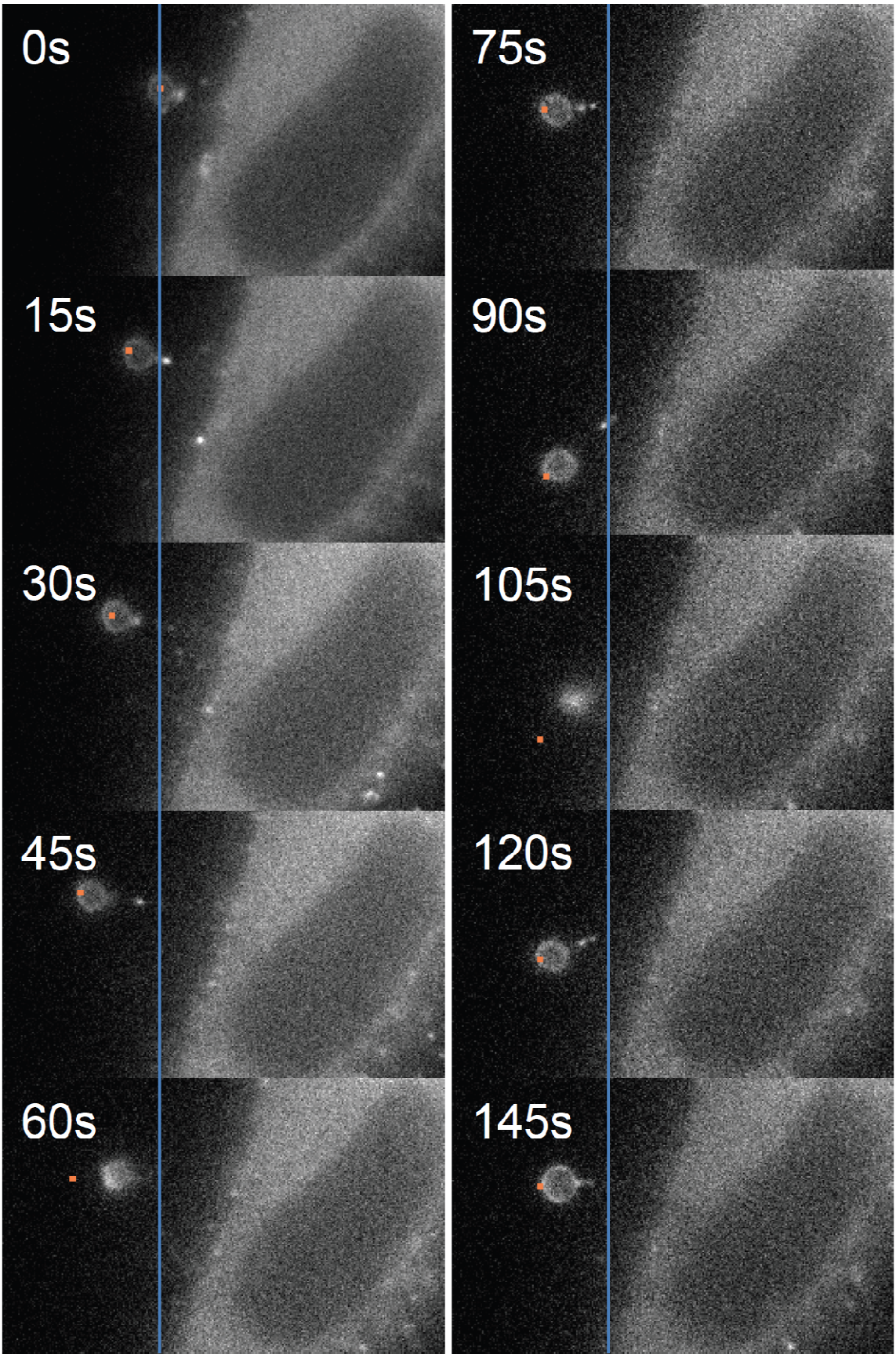
0s
15s
30s
45s
60s
75s
90s
105s
120s
145s

Figure 3.5. Filopodial attachments can be pulled away from the Myo10-labeled tip spot

Individual frames from a series of timelapse fluorescence microscope images of a HeLa cell transiently transfected with GFP-Myo10. A 4 um polystyrene bead is manipulated by an optical trap, the center of which is labeled by an orange square. The blue line running through all of the images indicates the starting position of the bead. Note that at 45s, and again at 90s, the bead is extended a small distance from the Myo10 tip spot. As the optical trap is pulled further from the cell body, the bead eventually springs back toward the cell (60s and 105s), indicating that the bead has remained attached to the filopodium, despite becoming dissociated from the apparent tip spot. In these experiments, the optical trap remains fixed while the stage is maneuvered. Images have been manually registered so that the sample appears fixed while the optical trap moves.

attachment with the bead, instead remaining relatively stationary within the filopodium while the point of attachment was pulled away. Once the filopodium was stretched too much, the force that it exerted on the bead exceeded the force of the optical trap, causing the filopodium and attached bead to recoil back towards the cell body. This behavior confirms that the bead does indeed stay attached despite the apparent distance between the bead and the initial tip spot. The bead could then be re-trapped and the filopodium re-extended with the same result: the point of attachment could be pulled some distance away from the distinct Myo10 tip spot for several seconds.

This separation of the induced filopodial attachment and the Myo10-enriched tip complex is quite intriguing because it suggests that the large cluster of Myo10 is neither bound directly to the attachment site, nor is it necessary for continued function, once it has formed. This result does not, however, discount the possibility that Myo10 is involved in the formation of the attachment. In our preliminary experiments, we used uncoated beads, which may adhere to filopodia nonspecifically, perhaps bypassing a Myo10-dependent adhesion. Beads coated in ECM proteins like fibronectin or vitronectin could be used to assay integrin-specific adhesions. It is also possible that some Myo10, albeit an undetectable quantity, does remain directly attached to the bead adhesion while the bulk of the Myo10 remains in filopodial shaft, perhaps bound to the end of the actin bundle. Future experiments could probe this possibility further using more sensitive imaging techniques, such as longer exposures or a Myo10 construct tagged with multiple fluorophores.

While our preliminary optical trap experiments do not provide definitive conclusions, it is clear that this represents a promising approach for a filopodial adhesion

assay. The ability to measure adhesion forces in several filopodia per cell could yield the kind of quantifiable data that may be necessary to parse the subtle contributions of several adhesion components. For example, in future experiments, we could knock down endogenous Myo10 and replace it with a construct lacking the FERM domain. The FERM-less Myo10 construct still induces filopodia, but is unable to bind to integrins (Bohil et al., 2006). Though some endogenous Myo10 would remain in these filopodia, we would expect a reduction in the strength of the adhesions because much of the Myo10 at tips would be incapable of delivering integrins or securing them directly to actin.

Actin-destabilizing drugs and FRAP

Myo10 is thought to maintain its localization to filopodial tips by continuing to migrate along the constantly polymerizing filopodial actin bundle. Our model also predicts that if Myo10 is bound to membrane proteins, like integrins, it will remain localized to sites of adhesion even when actin is removed. In unpublished experiments by Aparna Bohil, a stream of PBS was used to forcefully "blow off" HeLa cells from coverslips to which they had adhered, leaving behind plaques that were formerly filopodial tip spots and that clearly contained Myo10. This is consistent with the proposed adhesive abilities of filopodial tips and suggests that Myo10 is strongly anchored to these adhesions.

To test whether Myo10 localizes to sites of adhesion in the absence of actin, we imaged GFP-Myo10-expressing HeLa cells treated with the actin destabilizing drugs latrunculin B or cytochalasin D. Both drugs prevent the continued polymerization of actin by either sequestering actin monomers, in the case of latrunculin B, or capping actin

filaments, in the case of cytochalasin D. Treatment with 1 uM concentrations of either drug for 5 minutes causes the retraction of filopodial actin bundles at the rate of actin retrograde flow. This obviously results in a dramatic loss of all unattached filopodia, but many of the attached filopodia survive drug treatment. In some of these remaining filopodia, the Myo10 tip spot spread, also at the rate of actin retrograde flow (Figure 3.6). This spreading of the tip spot suggests that the filopodial tip complex is not a cohesive structure that remains anchored to either the end of the actin bundle or the site of adhesion. Instead, the tip complex appears to have a fluid nature and is likely the result of Myo10 running off of the end of the actin bundle and diffusing within the hollow space that is left when the actin retracts.

These results do not exclude the possibility that Myo10 is bound to a membrane protein, only that the bulk of Myo10 does not appear to be anchored to a filopodial tip adhesion. Indeed, one possibility is that as the actin retracts, Myo10 is becoming deposited at filopodial shaft adhesions. To determine whether this pool of Myo10 is fluid and diffusive in nature or is anchored and immobile, we performed fluorescence recovery after photobleaching (FRAP) on spread tip spots. Preliminary results indicate that, when a small portion in the middle of one of these spread tips is bleached, fluorescence recovers very rapidly and from both directions (base and tip) of the filopodium (Figure 3.6). This strongly indicates that Myo10 is diffusing freely within this space, but does not yet allow us to differentiate between a cytoplasmic or membrane-bound pool of Myo10. We predict that membrane-bound proteins would diffuse more slowly than cytoplasmic proteins, so it may be informative to compare Myo10's diffusion rates to

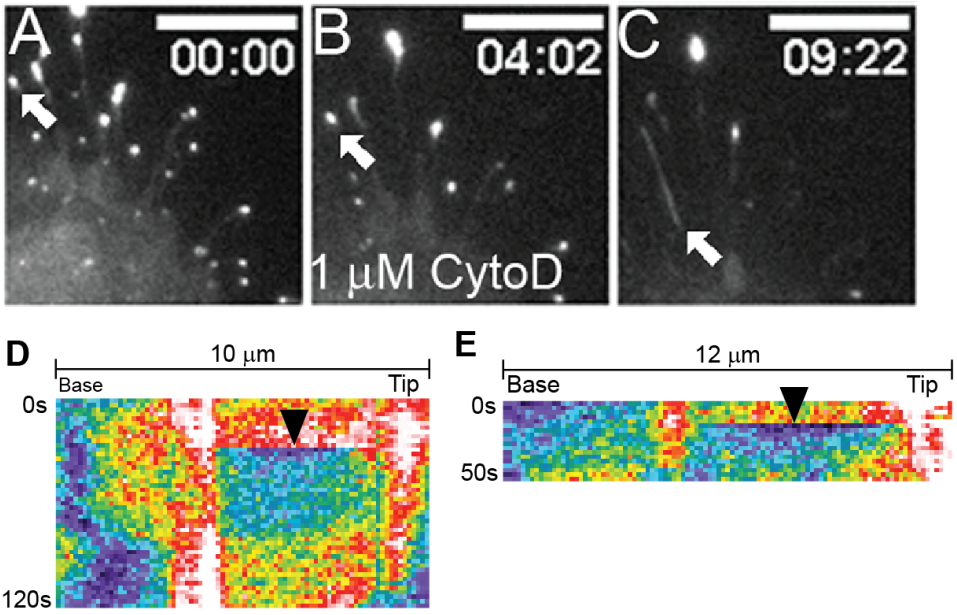

Figure 3.6. Myo10 clusters behave like fluids after cytochalasin D treatment

(**A-C**) Frames from a timelapse in which HeLa cells transfected with GFP-Myo10 are treated with 1 uM cytochalasin D. White arrow shows a tip spot that has spread after drug treatment. Also note the significant loss of unattached filopodia after cytochalasin D treatment. Scale bar represents 5 um. (**D-E**) Example kymographs of spread tip spots that have been photobleached at the time and location indicated by the black arrow. Kymographs are displayed as heatmaps in which white/red represent highest intensity and blue/black represent lowest intensity. Images (**A-C**) provided by Omar Quintero.

those of GFP-alone, which would act as a cytoplasmic marker; and GFP-GPI, a membrane marker.

Discussion

Myo10 is important in filopodial formation, but its role in filopodial function has been difficult to establish. Based on its localization, movement, and binding partners, Myo10 has been proposed as an intrafilopodial transporter and/or a membrane-cytoskeleton linker. We have attempted to test both possibilities.

We obtained few examples of integrins exhibiting intrafilopodial motility. This is perplexing, considering their reported enrichment at filopodial tips and the sensitivity of our imaging system (Zhang et al., 2004). In previous studies, beads that were linked to integrins via antibodies were reported to undergo rapid forward movement in growth cone filopodia, occasionally persisting for several microns (Grabham et al., 2000). Must integrins be activated by binding to an extracellular ligand before they can engage the filopodial transport machinery? This possibility does not fit well in models of pathogen capture or cell migration, which one assumes would apply a rearward pulling force on engaged integrins, not transport them towards filopodial tips. Another possibility is that the bond between Myo10 and integrins is relatively weak and transient and that the constant stream of Myo10 molecules causes integrins to be dragged in short spurts along the filopodium. This forward drag could be balanced by occasionally linking to proteins like talin, which would couple integrins to the rearward-flowing actin. Such a transport system would cause the integrins to be localized more evenly along the filopodial shaft, which is the localization pattern we typically observe in HeLas, making filopodia

uniformly sticky, not just at the tip. Of course, Myo10's relationship with integrins does not discount the possibility that it transports other proteins in filopodia.

Although our data do not put into question Myo10's status as a transporter, its role as a structural component of a putative tip complex has become tenuous. When sites of adhesion are pulled away from the tip complex, it does not always track with the adhesion. The tip complex also appears to be fluid in nature, which undermines its identity as a specialized, force-bearing anchor for the cell. These observations suggest a model in which filopodia are uniformly sticky and substrate adhesions stabilize the filopodia, allowing for the recruitment of focal adhesion proteins. As filopodial adhesions move towards the cell body, either by coupling to retrograde flow or by forward migration of the cell, they mature into focal adhesions. Myo10's role in this process may be to bias the localization of some proteins towards filopodia, but not to serve as the main integrin-cytoskeleton linker.

It is important to note that in the experiments described here, we use HeLa cells due to their many advantages. In addition to being convenient to culture and transfect, HeLas are also the cell type in which Myo10 is best characterized. HeLas also normally produce a high number of filopodia. But not all filopodia are created equal. Indeed, the structures that we refer to collectively as filopodia display an impressive amount of variety in their lengths, biophysical properties, and likely function, depending on cell type. The short "microspikes" in some growth cones, for example, do not typically bend and wave like the much longer and more dynamic filopodia of HeLas. Considering the amount of morphological variation, it is certainly reasonable to assume that filopodia are equally diverse in composition. This likelihood necessitates the comparison of different

cell types in future studies to determine which components are specific for certain cell types. Whether Myo10 powers a universal transport system in these disparate cell types remains to be seen.

Materials and Methods

Cells

HeLa cells were transfected with Polyfect (Qiagen) unless indicated otherwise. To obtain the relatively low levels of expression required to facilitate single-molecule imaging, HeLa cells were transfected for no more than 6-12 hours, unless otherwise stated. Cells were replated onto #1.5 glass coverslips or glass-bottom dishes (MatTek). Coverslips were precoated by incubating acid-washed coverslips for 20 minutes in 10 µg/ml fibronectin or vitronectin in PBS and then washed at least 3x in PBS over 10 minutes prior to plating. To minimize background from cellular debris, cells were usually plated onto coverslips at <10% confluence, with best results obtained with less than one cell per camera field. Cells were allowed to attach to the coverslip for 1-2 hours, unless otherwise stated, and the coverslip was mounted in a Rose chamber with a 3 mm spacer and a #1.5 coverslip for the roof. The chamber was completely filled with Optimem (Gibco). Tet-off HeLa cells (Clontech) that "stably" express GFP-Myo10 were generated as per the manufacturer's instructions. These cells were withdrawn from doxycycline for 1 day to induce expression of GFP-Myo10 and then plated onto glass coverslips and imaged as described above. Only a subset cells expressed detectable GFP-Myo10 following doxycycline withdrawal. For drug treatment experiments, 1 uM

concentration Latrunculin B or Cytochalasin D was flushed into custom Rose chambers during imaging.

TIRF

Objective type TIRF was performed as described in Kerber et al. The imaging system used here included an Andor IXON 897 EMCCD camera, which is much more sensitive than the Hamamatsu ORCA-ER used in Kerber et al. A 100X, 1.49NA TIRF objective lens was also used here in place of a 60X objective.

CALI

Cells were plated on fibronectin to encourage integrin-dependent adhesions. The CALI imaging protocol used here is described in Vitriol et al. We used an argon Spectra Physics Stabilite 2017 laser with a 400 mW, 488 nm line tuned to ~2.5 um at the sample plane. To achieve CALI, the sample was excited with a 100 msec pulse of laser light. We used either a 60X or 100X objective lens and captured images using a Sensicam QE camera. Temperature was maintained at 37C using a custom heating chamber that also allowed 5% CO2 to be flowed into the chamber. Metamorph software was used to control the microscope and acquire images.

Optical tweezers

An optical trap microscopy system was used to manipulate polystyrene or glass beads of either 2 um or 4 um in diameter. The location of the optical trap remained fixed while the position of the stage was manipulated to move the trapped beads relative to the

sample. Cells were imaged at video framerates using either brightfield illumination or fluorescence. Custom software was used to control the microscope and acquire images.

FRAP

Immunofluorescence samples were imaged on an Olympus FLUOVIEW FV 1000 inverted confocal microscope (Center Valley, PA) with a PlanApo 60X oil, 1.42 NA objective lens (UNC-Olympus Imaging Research Center). The FV1000 has diode lasers for 405 nm, 559 nm and 635 nm wavelengths, and an Argon laser for 488 nm wavelength use. For z-stacks, 0.2 um slices were collected at 4.0 us/pixel sampling speed in sequential line mode and using Kalman integration. For FRAP, the 405 nm line was used at 1-7% power to bleach regions of interest while images were simultaneously and continuously acquired using the 488 nm line.

Chapter 4: Conclusions and Future Directions

Summary

Despite much recent advancement in the study of Myo10's biophysical and cell biological properties, some questions persist. Is Myo10 a dimer? Does it transport cargo? How is it regulated? In this chapter, I will summarize the results presented in previous chapters while explaining their significance within the broader context of the field. I will also propose methods and materials that may allow for the development of an imaging system capable of tracking two colors with single-molecule sensitivity. Next, I will propose experiments that would use this two-color, single-molecule system to clarify Myo10's dimerization status and test for cargo transport. Finally, I will discuss the advantages of using single-molecule imaging in filopodia to study other motors that localize to actin-based protrusions.

Myo10 intrafilopodial motility

Movements of bright puncta of GFP-Myo10 were first described by Berg and Cheney (Berg and Cheney, 2002). These bright puncta often appear to originate as part or all of the Myo10 tip spot, which can be detected moving rearward quite often. Forward movements of these puncta back towards the tips (~80 nm/s) were much less common and most tips would refill with GFP-Myo10 via an undetectable mechanism.

Chapter 2 of this thesis adds some intriguing pieces to this puzzle. We discovered a population of Myo10 that likely represents single-molecules or dimers and moves frequently and with high velocity (578 +/- 174 nm/s) towards filopodial tips (Kerber et al., 2009). This finding has now been confirmed by the Ikebe group using similar methods, coincidentally measuring an identical 578 nm/s average forward velocity of Myo10 (Watanabe et al., 2010). They also reported evidence of two-step photobleaching of these faint particles, suggesting that the fast moving population of Myo10 consists of dimers. Based on my own measurements, the bright puncta of Myo10 are roughly 50-100 times brighter than the intensity of a single GFP-Myo10 molecule. Taken together, this data provides very clear evidence that Myo10 undergoes intrafilopodial movement as part of a larger cluster and as a single unit.

Why are there two distinct populations of Myo10 that exhibit different modes of intrafilopodial movement? In our working model, Myo10 dimers move towards and accumulate at filopodial tips. Possibly triggered by a regulatory signal, or perhaps as a result of overcrowding, these clusters of Myo10 occasionally couple to the retrograde flow of the filopodial actin. This rearward movement of Myo10 clusters may represent a recycling mechanism or a means of transporting cargo from filopodia to the cell body. Occasional forward movements of these bright puncta may be a result of some Myo10's in the cluster becoming reactivated.

It should be noted that, although Myo10 is capable of migrating along the sides of actin filaments and bundles (Nagy et al., 2008), the movements exhibited in filopodia may represent Myo10 particles riding the barbed ends of new filaments as they enter and grow within an existing filopodium. In preliminary experiments, we imaged a

constitutively active form of a protein called formin, which is known to associate with the polymerizing, barbed ends of actin filaments (Campellone and Welch, 2010). We detected formin particles moving along the leading edge of HeLa cells and occasionally entering filopodia, where they continued to move in a directed fashion towards the filopodial tip (Figure 4.1). Interestingly, we measured the average speed of formins in filopodia to be roughly 570 nm/s. These provocative observations raise the possibility that Myo10's movement may rely on the polymerization of new actin filaments rather than the sides of existing filaments. The addition of new actin filaments to existing filopodia would also represent a novel mechanism of filopodial maintenance.

Myo10 as a potential cargo transporter

Myo10's distinct forward and rearward movement in filopodia, combined with its ability to bind to proteins like integrins, led to the hypothesis that it functions as an intrafilopodial transporter (Berg and Cheney, 2002). An analogous system of transport in flagella, which are microtubule-based protrusions, has now been implicated in several human diseases (Badano et al., 2006; Rosenbaum and Witman, 2002). While intraflagellar transport is powered by the forward and rearward movements of kinesin and dynein motors, transport in filopodia could be powered by Myo10 forward movement and actin retrograde flow.

Compelling evidence for a filopodial transport system remains mostly correlative. Some of Myo10's binding partners, like VASP and integrins, have been reported to colocalize at filopodial tips (Tokuo and Ikebe, 2004; Zhang et al., 2004). In addition, we were able to detect a population of faint VASP particles moving forward in filopodia at

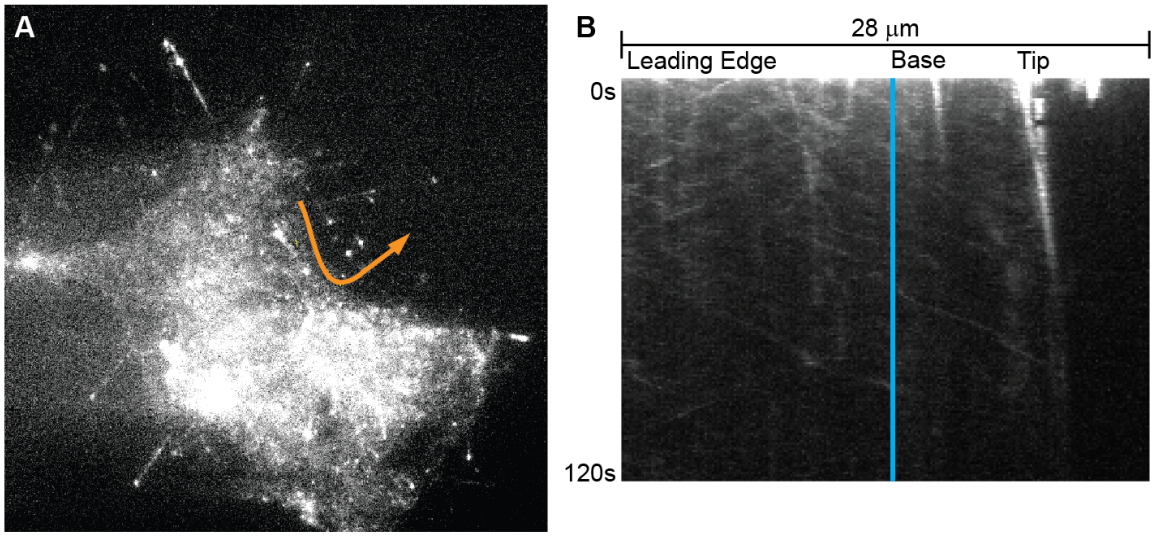

Figure 4.1. Single molecules of formin exhibit fast forward movement in filopodia

(**A**) HeLa cell overexpressing a constitutively active version of formin, GFP-mDia2(ΔGBD), and imaged using single-molecule TIRF. Orange arrow indicates the path kymographed in (**B**). The left half of the kymograph follows the leading edge of the cell. Tracks in this part of the kymograph represent formin molecules moving parallel to the edge of the cell. The criss-crossing pattern indicates that formin moves in both directions along the edge, seemingly crossing paths often. The cyan line indicates the approximate border between the cell edge (left) and the filopodium (right). Note that particles appear to move only in the forward direction once they enter the filopodium in this example. Importantly, velocities remain constant, whether formin is moving at the cell edge or within the filopodium.

speeds virtually identical to that of Myo10 (Kerber et al., 2009). Likewise, integrin-bound beads were reported to move forward at ~600 nm/s in growth cone filopodia (Grabham et al., 2000).

In Chapter 3 of this thesis, we described initial experiments intended to investigate whether Myo10 functions as a cargo transporter in filopodia. Although definitive conclusions should not be drawn from these preliminary results, there were several provocative observations. Despite repeated attempts to detect frequent, fast movement of $\alpha5\beta1$ and $\alpha V\beta3$ integrins in filopodia, we observed only a few short spurts of forward movement. This may have been due to a deficiency in our imaging protocol, or it may hint at a type of intrafilopodial transport that is more subtle than was originally hypothesized. It is also possible that integral membrane proteins like integrins or DCC, to which Myo10 also binds (Wei et al., 2011), are transported differently than cytoplasmic proteins like VASP. Direct visualization of intrafilopodial motility, however, remains a promising method for identifying new candidate cargos of Myo10. Ideally, future experiments will be able to demonstrate Myo10 and cargo cotransport at the single-molecule level, but this will require us to overcome several technical challenges.

The challenges of single-molecule tracking in two colors

Filopodia provide an ideal environment for single-molecule studies in living cells. They are far from the autofluorescent glow of the cell body, immobilized on the substrate, and are essentially one-dimensional tracks. Although genetically encoded fluorophores provide some key advantages, they also come with serious drawbacks.

Even GFP, the brightest and longest-lasting of the fluorophores currently available, does not fluoresce with a steady intensity, occasionally blinking "off" entirely. Even when "on," an individual GFP molecule is quite dim and bleaches rapidly compared to non-peptide fluorophores like quantum dots. Despite these shortcomings, we were able to successfully track GFP-labeled Myo10 in living cells with single-molecule sensitivity. Attempts to perform the same feat with mCherry-Myo10 have so far proven ineffective. Red fluorophores, like mCherry, are even dimmer and bleach faster than GFP. This particular obstacle may be resolved with relative ease by creating a Myo10 construct that is tagged with improved or multiple red fluorophores, such as TagRFP (Merzlyak et al., 2007). Our lab now possesses a 3X-TagRFP DNA construct that can be used for cloning with our existing library of Myo10 constructs, making red versions of Myo10 that could be successfully tracked at the single-molecule level.

Another way to boost the light emitted from fluorophores is to increase the power of the excitation light. Under our normal imaging conditions, we perform total internal reflection fluorescence (TIRF) microscopy by exciting our samples with 40 mW laser light. The laser that we currently use to excite red fluorophores is less powerful, sending 20 mW into our microscope. More powerful lasers would increase the amount of light emitted from each fluorophore, making detection easier. This increase in signal would allow us to decrease exposure times and increase acquisition framerates, which is another challenge for tracking in two colors. Capturing images in two colors would require us to capture twice as many images in the same amount of time in order to maintain the same framerates. The camera that we used for the initial imaging studies, a Hamamatsu ORCA ER, is incapable of capturing images at that rate. Fortunately, we now possess a camera,

an Andor IXON 897, that can acquire images at much higher framerates. This camera has the added advantages of having a back-thinned, super-cooled, EMCCD chip, which means that it is more sensitive and can also amplify signals. The final challenge to tracking faint spots is that most available software is incapable of successfully following spots that are difficult to distinguish from background and that blink on and off. We have developed a spot-tracking software program that exploits the one-dimensional path to which our spots are restricted and has proven capable of tracking single molecules.

Kymotracker

In Chapter 2, we introduced a novel concept for using kymography to aid in the automatic tracking of extremely faint spots in timelapse video data. The concept was simple: although fast-moving, single molecules are notoriously difficult to track due to their dimness and blinking, kymographs are able to display the coordinates of these molecules over time because their paths (filopodia) are well defined. Even dim particles moving along these paths create clear tracks in a kymograph regardless of blinking, essentially mapping the exact location vs. time of all particles along the path. By using the kymograph tracks as coordinates to seed a spot-finding algorithm, we were able to very accurately track single molecules and perform automated measurements of intensity, centroid position, and velocity in every frame of the original timelapse data. Our program, named Kymotracker, was written in Python and currently runs in either the Linux or Windows operating environments. This powerful spot-tracking method would be relatively simple to incorporate into existing software, however, and is potentially a boon for the imaging of any faint particles moving on a defined path. For example,

current in vitro studies of myosin motors involve the imaging of purified motors along immobilized actin filaments and future in vivo studies of stereocilia motors and cargos may take advantage of the relatively convenient system of HeLa cell filopodia.

Directly visualization of Myo10 dimerization and cargo transport

Development of a single-molecule imaging system capable of tracking two colors in live cells would represent an important advancement in cell biology and biophysics in general. Obviously, this system would also serve as a powerful tool to probe Myo10 specifically. Our model of Myo10 predicts that single-molecule imaging experiments would reveal Myo10 dimers moving in lock-step with cargo molecules. Direct visualization of coordinate movement of red and green dimers of Myo10 in filopodia would beautifully and convincingly illustrate one of the most fundamental properties of Myo10. To test whether the Myo10 α-helical region is facilitating dimerization, we could swap it for the α-helical regions of myosins known to be either monomers or dimers. If Myo10 is converted into a monomer, it may be incapable of any intrafilopodial motility or localization. Since the length of Myo10's lever arm may be extended by its α-helical region, and this length is thought to partially dictate its selectivity for bundled actin, it would be interesting to see whether the α-helical regions of other myosins would alter Myo10's velocity in filopodia or cause it to prefer other actin structures (Nagy and Rock, 2010). To test whether the α-helical region of Myo10 is sufficient to induce dimerization or selectivity for filopodial actin, we could swap it into a known monomeric myosin, or one known to localize to other types of actin.

The direct visualization of Myo10 and cargo at the single-molecule level could provide novel insights into the nature of the intrafilopodial transport system. For example, does Myo10 provide a non-stop flight to the filopodial tip, or are there layovers on the way, where its passengers are exchanged? So far, the single-molecule tracks produced by VASP suggest that it travels in a non-stop fashion towards filopodial tips. Integrins, however, may hop on and off of frequently, spending the rest of their time meandering aimlessly along the filopodial membrane. Tracking vehicles and cargos simultaneously may allow us to distinguish between these and other, perhaps unforeseen modes of transport. The ability to assay for cotransport would also allow us to determine which domains of Myo10 are responsible for binding to its various cargos. We currently possess a library of Myo10 truncation constructs that could be used to test which domains are necessary or sufficient for cotransport.

Filopodia: an ideal environment for studying stereocilia motors and cargos

Advancements in imaging Myo10 in filopodia may also provide powerful tools for studying the motors that function in other filopodia-like structures, such as stereocilia. Stereocilia are similar to filopodia in that they are slender cellular protrusions with tightly-packed actin bundles at their cores (Tilney et al., 1980). Rearward actin flow in these structures is also much slower than is typical for filopodia (Rzadzinska et al., 2004). Stereocilia contain a specific set of myosin motors, including myosin-IIIa, VI, and the MyTH4-FERM myosins, VIIa and XVa. Naturally occurring mutations in these myosins are known to cause inherited deafness (Friedman et al., 1999; Walsh et al., 2002). Intriguingly, myosin-IIIa localizes to filopodial tips and is required for the localization of

espin, an actin-bundling protein also implicated in deafness, to stereocilia tips (Salles et al., 2009; Zheng et al., 2000). Likewise, myosin-XVa localizes to filopodial tips and is required for the localization of whirlin and eps8 to the tips of stereocilia (Belyantseva et al., 2005; Manor et al., 2011). In humans, a mutation that eliminates whirlin's PDZ domain, which is thought to link it to myosin-XVa, is also associated with deafness (Mburu et al., 2003). Eps8 is thought to regulate the length of stereocilia and mice lacking eps8 are deaf. Future studies of these motors and their cargos could benefit from using filopodia and single-molecule imaging.

Our lab has obtained GFP-labeled constructs of myosin-IIIa, and myosin-XVa (generously provided by Beth Burnside at UC Berkeley and Tom Friedman at the NIH, respectively). I have transfected HeLa cells with either GFP-Myo3a (delta kinase) or GFP-Myo15a and imaged them using our TIRF system. Preliminary results show that GFP-Myo3a accumulates at filopodial tips while GFP-Myo15a localizes partially to tips, but also along the lengths of filopodia (Figure 4.2). Our preliminary attempts to track these motors produced kymograph tracks that hint at directed movement, but we did not detect clear, long-range forward movements like those of Myo10. It is possible that the increased localization of these motors to the shafts of filopodia creates background fluorescence against which it is difficult to see single molecules moving. It is also possible that these motors are monomers, while Myo10 may be a dimer and potentially twice as bright. Finally, if these motors move too fast, our current imaging system may be unable to detect them.

The combination of TIRF and filopodia may represent the ideal system for studying the interaction of similar motors and their cargos in the context of a living cell.

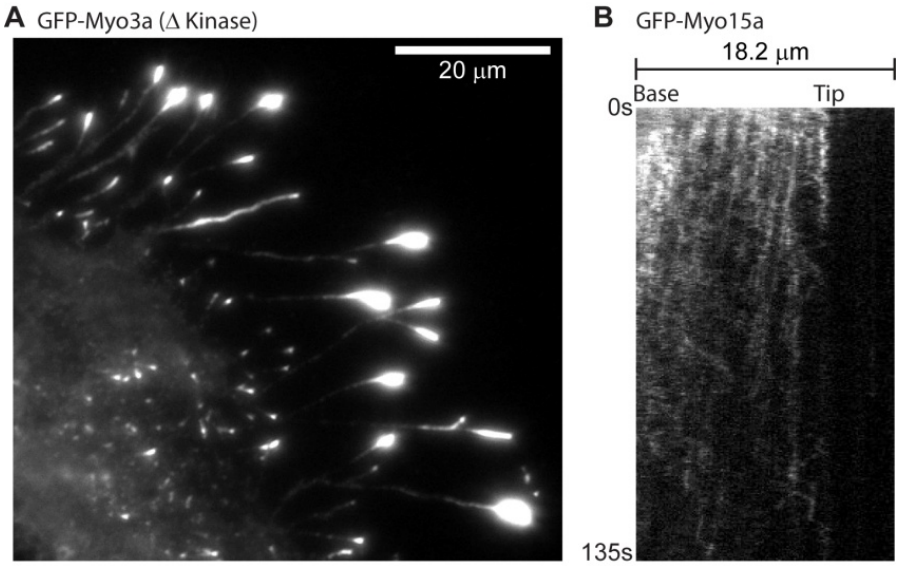

Figure 4.2. Deafness myosins localize to filopodial tips and may display intrafilopodial motility

(**A**) TIRF image of a HeLa cell transfected with GFP-Myo3a (delta Kinase). Note the clear accumulation at filopodial tips. (**B**) Kymograph of a filopodium from a cell transfected with GFP-Myo15a. Note that, although many tracks appear to overlap and make it difficult to analyze any single particle, there are several clear examples of slow rearward tracks as well as possible fast forward tracks.

In the case of stereociliar motors and cargos, the use of established cell lines like HeLa or Cos-7 cells would be much easier than using primary cells dissected from the inner ear of an animal. Since stereociliar motors are only expressed in the inner ear, HeLas and Cos-7 cells would provide natural knockout-like cell lines for these studies. The existence of a myosin-powered transport system in stereocilia suggests that directed, long-range transport along bundled actin structures is a conserved phenomenon. Myo10 still represents the most likely candidate for powering a ubiquitous, novel transport system specific to filopodia. Future research will be required to determine the in vivo functions of intrafilopodial motility and whether its physiological importance will rival that of intraflagellar transport.

References

Albrecht-Buehler, G., and R.D. Goldman. 1976. Microspike-mediated particle transport towards the cell body during early spreading of 3T3 cells. *Exp Cell Res*. 97:329-339.

Almagro, S., C. Durmort, A. Chervin-Petinot, S. Heyraud, M. Dubois, O. Lambert, C. Maillefaud, E. Hewat, J.P. Schaal, P. Huber, and D. Gulino-Debrac. 2010. The motor protein myosin-X transports VE-cadherin along filopodia to allow the formation of early endothelial cell-cell contacts. *Mol Cell Biol*. 30:1703-1717.

Baboolal, T.G., T. Sakamoto, E. Forgacs, H.D. White, S.M. Jackson, Y. Takagi, R.E. Farrow, J.E. Molloy, P.J. Knight, J.R. Sellers, and M. Peckham. 2009. The SAH domain extends the functional length of the myosin lever. *Proc Natl Acad Sci U S A*. 106:22193-22198.

Badano, J.L., N. Mitsuma, P.L. Beales, and N. Katsanis. 2006. The ciliopathies: an emerging class of human genetic disorders. *Annu Rev Genomics Hum Genet*. 7:125-148.

Belyantseva, I.A., E.T. Boger, S. Naz, G.I. Frolenkov, J.R. Sellers, Z.M. Ahmed, A.J. Griffith, and T.B. Friedman. 2005. Myosin-XVa is required for tip localization of whirlin and differential elongation of hair-cell stereocilia. *Nat Cell Biol*. 7:148-156.

Bennett, R.D., A.J. Caride, A.S. Mauer, and E.E. Strehler. 2008. Interaction with the IQ3 motif of myosin-10 is required for calmodulin-like protein-dependent filopodial extension. *FEBS Lett*. 582:2377-2381.

Bennett, R.D., A.S. Mauer, and E.E. Strehler. 2007. Calmodulin-like protein increases filopodia-dependent cell motility via up-regulation of myosin-10. *J Biol Chem*. 282:3205-3212.

Bennett, R.D., and E.E. Strehler. 2008. Calmodulin-like protein enhances myosin-10 translation. *Biochem Biophys Res Commun*. 369:654-659.

Berg, J.S., and R.E. Cheney. 2002. Myosin-X is an unconventional myosin that undergoes intrafilopodial motility. *Nat Cell Biol*. 4:246-250.

Berg, J.S., B.H. Derfler, C.M. Pennisi, D.P. Corey, and R.E. Cheney. 2000. Myosin-X, a novel myosin with pleckstrin homology domains, associates with regions of dynamic actin. *J Cell Sci*. 113:3439-3451.

Bohil, A.B., B.W. Robertson, and R.E. Cheney. 2006. Myosin-X is a molecular motor that functions in filopodia formation. *Proc Natl Acad Sci U S A*. 103:12411-12416.

Brawley, C.M., and R.S. Rock. 2009. Unconventional myosin traffic in cells reveals a selective actin cytoskeleton. *Proc Natl Acad Sci U S A*. 106:9685-9690.

Burridge, K., and P. Mangeat. 1984. An interaction between vinculin and talin. *Nature*. 308:744-746.

Campellone, K.G., and M.D. Welch. 2010. A nucleator arms race: cellular control of actin assembly. *Nature reviews. Molecular cell biology*. 11:237-251.

Chen, L., F. Wang, H. Meng, and J.R. Sellers. 2001. Characterization of Recombinant Myosin X. *Biophys J (Annual Meeting Abstracts)*. 80:573a.

Chishti, A.H., A.C. Kim, S.M. Marfatia, M. Lutchman, M. Hanspal, H. Jindal, S.C. Liu, P.S. Low, G.A. Rouleau, N. Mohandas, J.A. Chasis, J.G. Conboy, P. Gascard, Y. Takakuwa, S.C. Huang, E.J. Benz, Jr., A. Bretscher, R.G. Fehon, J.F. Gusella, V. Ramesh, F. Solomon, V.T. Marchesi, S. Tsukita, K.B. Hoover, and et al. 1998. The FERM domain: a unique module involved in the linkage of cytoplasmic proteins to the membrane. *Trends Biochem Sci*. 23:281-282.

Cox, D., J.S. Berg, M. Cammer, J.O. Chinegwundoh, B.M. Dale, R.E. Cheney, and S. Greenberg. 2002. Myosin X is a downstream effector of PI(3)K during phagocytosis. *Nat Cell Biol*. 4:469-477.

Dent, E.W., and F.B. Gertler. 2003. Cytoskeletal dynamics and transport in growth cone motility and axon guidance. *Neuron*. 40:209-227.

Dent, E.W., A.V. Kwiatkowski, L.M. Mebane, U. Philippar, M. Barzik, D.A. Rubinson, S. Gupton, J.E. Van Veen, C. Furman, J. Zhang, A.S. Alberts, S. Mori, and F.B. Gertler. 2007. Filopodia are required for cortical neurite initiation. *Nat Cell Biol*. 9:1347-1359.

Divito, M.M., and R.E. Cheney. 2008. Myosin10. *In* Myosins: A Superfamily of Molecular Motors. L.M. Coluccio, editor. Springer. 403-419.

Dubash, A.D., M.M. Menold, T. Samson, E. Boulter, R. Garcia-Mata, R. Doughman, and K. Burridge. 2009. Chapter 1. Focal adhesions: new angles on an old structure. *Int Rev Cell Mol Biol*. 277:1-65.

Eilken, H.M., and R.H. Adams. 2010. Dynamics of endothelial cell behavior in sprouting angiogenesis. *Current opinion in cell biology*. 22:617-625.

Faix, J., and K. Rottner. 2006. The making of filopodia. *Curr Opin Cell Biol*. 18:18-25.

Friedman, A.L., M.A. Geeves, D.J. Manstein, and J.A. Spudich. 1998. Kinetic characterization of myosin head fragments with long-lived myosin.ATP states. *Biochemistry*. 37:9679-9687.

Friedman, T.B., J.R. Sellers, and K.B. Avraham. 1999. Unconventional myosins and the genetics of hearing loss. *Am J Med Genet*. 89:147-157.

Grabham, P.W., M. Foley, A. Umeojiako, and D.J. Goldberg. 2000. Nerve growth factor stimulates coupling of beta-1 integrin to distinct transport mechanisms in the filopodia of growth cones. *J Cell Sci*. 113:3003-3012.

Hermann, P., M. Armant, E. Brown, M. Rubio, H. Ishihara, D. Ulrich, R.G. Caspary, F.P. Lindberg, R. Armitage, C. Maliszewski, G. Delespesse, and M. Sarfati. 1999. The vitronectin receptor and its associated CD47 molecule mediates proinflammatory cytokine synthesis in human monocytes by interaction with soluble CD23. *The Journal of cell biology*. 144:767-775.

Homma, K., and M. Ikebe. 2005. Myosin X is a high duty ratio motor. *J Biol Chem*. 280:29381-29391.

Homma, K., J. Saito, R. Ikebe, and M. Ikebe. 2001. Motor function and regulation of myosin X. *J Biol Chem*. 276:34348-34354.

Horwitz, A., K. Duggan, C. Buck, M.C. Beckerle, and K. Burridge. 1986. Interaction of plasma membrane fibronectin receptor with talin--a transmembrane linkage. *Nature*. 320:531-533.

Hu, K., L. Ji, K.T. Applegate, G. Danuser, and C.M. Waterman-Storer. 2007. Differential transmission of actin motion within focal adhesions. *Science*. 315:111-115.

Huang, X., and J.P. Saint-Jeannet. 2004. Induction of the neural crest and the opportunities of life on the edge. *Developmental biology*. 275:1-11.

Hwang, Y.S., T. Luo, Y. Xu, and T.D. Sargent. 2009. Myosin-X is required for cranial neural crest cell migration in Xenopus laevis. *Dev Dyn*. 238:2522-2529.

Isakoff, S.J., T. Cardozo, J. Andreev, Z. Li, K.M. Ferguson, R. Abagyan, M.A. Lemmon, A. Aronheim, and E.Y. Skolnik. 1998. Identification and analysis of PH domain-containing targets of phosphatidylinositol 3-kinase using a novel in vivo assay in yeast. *Embo J*. 17:5374-5387.

Iwaki, M., H. Tanaka, A.H. Iwane, E. Katayama, M. Ikebe, and T. Yanagida. 2006. Cargo-binding makes a wild-type single-headed myosin-VI move processively. *Biophys J*. 90:3643-3652.

Jacobson, K., Z. Rajfur, E. Vitriol, and K. Hahn. 2008. Chromophore-assisted laser inactivation in cell biology. *Trends in cell biology*. 18:443-450.

Kerber, M.L., D.T. Jacobs, L. Campagnola, B.D. Dunn, T. Yin, A.D. Sousa, O.A. Quintero, and R.E. Cheney. 2009. A Novel Form of Motility in Filopodia Revealed by Imaging Myosin-X at the Single-Molecule Level. *Curr Biol*.

Knight, P.J., K. Thirumurugan, Y. Xu, F. Wang, A.P. Kalverda, W.F. Stafford, 3rd, J.R. Sellers, and M. Peckham. 2005a. The predicted coiled-coil domain of myosin 10 forms a novel elongated domain that lengthens the head. *J Biol Chem*. 280:34702-34708.

Knight, P.J., K. Thirumurugan, Y. Yu, F. Wang, A.P. Kalverda, W.F. Stafford, 3rd, J.R. Sellers, and M. Peckham. 2005b. The predicted coiled-coil domain of myosin 10 forms a novel elongated domain that lengthens the head. *J Biol Chem*. 280:34702-34708.

Koleske, A.J. 2003. Do filopodia enable the growth cone to find its way? *Sci STKE*. 2003:pe20.

Kovacs, M., F. Wang, and J.R. Sellers. 2005. Mechanism of action of myosin X, a membrane-associated molecular motor. *J Biol Chem*. 280:15071-15083.

Kress, H., E.H. Stelzer, D. Holzer, F. Buss, G. Griffiths, and A. Rohrbach. 2007. Filopodia act as phagocytic tentacles and pull with discrete steps and a load-dependent velocity. *Proc Natl Acad Sci U S A*. 104:11633-11638.

Kwon, M., S.A. Godinho, N.S. Chandhok, N.J. Ganem, A. Azioune, M. Thery, and D. Pellman. 2008. Mechanisms to suppress multipolar divisions in cancer cells with extra centrosomes. *Genes Dev*. 22:2189-2203.

Lehmann, M.J., N.M. Sherer, C.B. Marks, M. Pypaert, and W. Mothes. 2005. Actin- and myosin-driven movement of viruses along filopodia precedes their entry into cells. *J Cell Biol*. 170:317-325.

Liao, J.C., J. Roider, and D.G. Jay. 1994. Chromophore-assisted laser inactivation of proteins is mediated by the photogeneration of free radicals. *Proceedings of the National Academy of Sciences of the United States of America*. 91:2659-2663.

Lidke, D.S., K.A. Lidke, B. Rieger, T.M. Jovin, and D.J. Arndt-Jovin. 2005. Reaching out for signals: filopodia sense EGF and respond by directed retrograde transport of activated receptors. *J Cell Biol*. 170:619-626.

Liu, J., D.W. Taylor, E.B. Krementsova, K.M. Trybus, and K.A. Taylor. 2006. Three-dimensional structure of the myosin V inhibited state by cryoelectron tomography. *Nature*. 442:208-211.

Macias, M.J., A. Musacchio, H. Ponstingl, M. Nilges, M. Saraste, and H. Oschkinat. 1994. Structure of the pleckstrin homology domain from beta-spectrin. *Nature*. 369:675-677.

Manor, U., A. Disanza, M. Grati, L. Andrade, H. Lin, P.P. Di Fiore, G. Scita, and B. Kachar. 2011. Regulation of stereocilia length by myosin XVa and whirlin depends on the actin-regulatory protein Eps8. *Current biology : CB*. 21:167-172.

Mashanov, G.I., D. Tacon, M. Peckham, and J.E. Molloy. 2004. The spatial and temporal dynamics of pleckstrin homology domain binding at the plasma membrane measured by imaging single molecules in live mouse myoblasts. *J Biol Chem*. 279:15274-15280.

Mattila, P.K., and P. Lappalainen. 2008. Filopodia: molecular architecture and cellular functions. *Nat Rev Mol Cell Biol*. 9:446-454.

Mburu, P., M. Mustapha, A. Varela, D. Weil, A. El-Amraoui, R.H. Holme, A. Rump, R.E. Hardisty, S. Blanchard, R.S. Coimbra, I. Perfettini, N. Parkinson, A.M. Mallon, P. Glenister, M.J. Rogers, A.J. Paige, L. Moir, J. Clay, A. Rosenthal, X.Z. Liu, G. Blanco, K.P. Steel, C. Petit, and S.D. Brown. 2003. Defects in whirlin, a

PDZ domain molecule involved in stereocilia elongation, cause deafness in the whirler mouse and families with DFNB31. *Nat Genet*. 34:421-428.

Medeiros, N.A., D.T. Burnette, and P. Forscher. 2006. Myosin II functions in actin-bundle turnover in neuronal growth cones. *Nat Cell Biol*. 8:215-226.

Merzlyak, E.M., J. Goedhart, D. Shcherbo, M.E. Bulina, A.S. Shcheglov, A.F. Fradkov, A. Gaintzeva, K.A. Lukyanov, S. Lukyanov, T.W. Gadella, and D.M. Chudakov. 2007. Bright monomeric red fluorescent protein with an extended fluorescence lifetime. *Nature methods*. 4:555-557.

Morgan, M.R., A. Byron, M.J. Humphries, and M.D. Bass. 2009. Giving off mixed signals--distinct functions of alpha5beta1 and alphavbeta3 integrins in regulating cell behaviour. *IUBMB Life*. 61:731-738.

Musacchio, A., T. Gibson, P. Rice, J. Thompson, and M. Saraste. 1993. The PH domain: a common piece in the structural patchwork of signalling proteins. *Trends Biochem Sci*. 18:343-348.

Nagy, S., B.L. Ricca, M.F. Norstrom, D.S. Courson, C.M. Brawley, P.A. Smithback, and R.S. Rock. 2008. A myosin motor that selects bundled actin for motility. *Proc Natl Acad Sci U S A*. 105:9616-9620.

Nagy, S., and R.S. Rock. 2010. Structured post-IQ domain governs selectivity of myosin X for fascin-actin bundles. *J Biol Chem*. 285:26608-26617.

Nambiar, R., R.E. McConnell, and M.J. Tyska. 2010. Myosin motor function: the ins and outs of actin-based membrane protrusions. *Cell Mol Life Sci*. 67:1239-1254.

Narasimhulu, S.B., and A.S. Reddy. 1998. Characterization of microtubule binding domains in the Arabidopsis kinesin-like calmodulin binding protein. *Plant Cell*. 10:957-965.

Nie, S., Y. Kee, and M. Bronner-Fraser. 2009. Myosin-X is critical for migratory ability of Xenopus cranial neural crest cells. *Dev Biol*. 335:132-142.

Odronitz, F., and M. Kollmar. 2007. Drawing the tree of eukaryotic life based on the analysis of 2,269 manually annotated myosins from 328 species. *Genome Biol*. 8:R196.

Oliver, T.N., J.S. Berg, and R.E. Cheney. 1999. Tails of unconventional myosins. *Cell Mol. Life Sci.* 56:243-257.

Park, H., B. Ramamurthy, M. Travaglia, D. Safer, L.Q. Chen, C. Franzini-Armstrong, P.R. Selvin, and H.L. Sweeney. 2006. Full-length myosin VI dimerizes and moves processively along actin filaments upon monomer clustering. *Mol Cell*. 21:331-336.

Partridge, M.A., and E.E. Marcantonio. 2006. Initiation of attachment and generation of mature focal adhesions by integrin-containing filopodia in cell spreading. *Molecular biology of the cell*. 17:4237-4248.

Phichith, D., M. Travaglia, Z. Yang, X. Liu, A.B. Zong, D. Safer, and H.L. Sweeney. 2009. Cargo binding induces dimerization of myosin VI. *Proc Natl Acad Sci U S A*. 106:17320-17324.

Pi, X., R. Ren, R. Kelley, C. Zhang, M. Moser, A.B. Bohil, M. Divito, R.E. Cheney, and C. Patterson. 2007. Sequential roles for myosin-X in BMP6-dependent filopodial extension, migration, and activation of BMP receptors. *J Cell Biol*. 179:1569-1582.

Pierce, D.W., N. Hom-Booher, and R.D. Vale. 1997. Imaging individual green fluorescent proteins [letter]. *Nature*. 388:338.

Plantard, L., A. Arjonen, J.G. Lock, G. Nurani, J. Ivaska, and S. Stromblad. 2010. PtdIns(3,4,5)P is a regulator of myosin-X localization and filopodia formation. *J Cell Sci*. 123:3525-3534.

Rechsteiner, M., and S.W. Rogers. 1996. PEST sequences and regulation by proteolysis. *Trends Biochem Sci*. 21:267-271.

Ricca, B.L., and R.S. Rock. 2010. The stepping pattern of myosin X is adapted for processive motility on bundled actin. *Biophys J*. 99:1818-1826.

Rogers, M.S., and E.E. Strehler. 2001. The tumor-sensitive calmodulin-like protein is a specific light chain of human unconventional myosin X. *J Biol Chem*. 276:12182-12189.

Rosenbaum, J.L., and G.B. Witman. 2002. Intraflagellar transport. *Nature reviews. Molecular cell biology*. 3:813-825.

Ross, J.L., M.Y. Ali, and D.M. Warshaw. 2008. Cargo transport: molecular motors navigate a complex cytoskeleton. *Curr Opin Cell Biol*. 20:41-47.

Rzadzinska, A.K., M.E. Schneider, C. Davies, G.P. Riordan, and B. Kachar. 2004. An actin molecular treadmill and myosins maintain stereocilia functional architecture and self-renewal. *J Cell Biol*. 164:887-897.

Salles, F.T., R.C. Merritt, Jr., U. Manor, G.W. Dougherty, A.D. Sousa, J.E. Moore, C.M. Yengo, A.C. Dose, and B. Kachar. 2009. Myosin IIIa boosts elongation of stereocilia by transporting espin 1 to the plus ends of actin filaments. *Nat Cell Biol*. 11:443-450.

Samuelsson, S.J., P.W. Luther, D.W. Pumplin, and R.J. Bloch. 1993. Structures linking microfilament bundles to the membrane at focal contacts. *The Journal of cell biology*. 122:485-496.

Schneider, M.E., A.C. Dose, F.T. Salles, W. Chang, F.L. Erickson, B. Burnside, and B. Kachar. 2006. A new compartment at stereocilia tips defined by spatial and temporal patterns of myosin IIIa expression. *J Neurosci*. 26:10243-10252.

Schoumacher, M., R.D. Goldman, D. Louvard, and D.M. Vignjevic. 2010. Actin, microtubules, and vimentin intermediate filaments cooperate for elongation of invadopodia. *J Cell Biol*. 189:541-556.

Scott, G., S. Leopardi, S. Printup, and B.C. Madden. 2002. Filopodia are conduits for melanosome transfer to keratinocytes. *J Cell Sci*. 115:1441-1451.

Sherer, N.M., M.J. Lehmann, L.F. Jimenez-Soto, C. Horensavitz, M. Pypaert, and W. Mothes. 2007. Retroviruses can establish filopodial bridges for efficient cell-to-cell transmission. *Nat Cell Biol*. 9:310-315.

Sherer, N.M., and W. Mothes. 2008. Cytonemes and tunneling nanotubules in cell-cell communication and viral pathogenesis. *Trends Cell Biol*. 18:414-420.

Singh, S.K., R. Kurfurst, C. Nizard, S. Schnebert, E. Perrier, and D.J. Tobin. 2010. Melanin transfer in human skin cells is mediated by filopodia--a model for homotypic and heterotypic lysosome-related organelle transfer. *FASEB J*. 24:3756-3769.

Sivaramakrishnan, S., B.J. Spink, A.Y. Sim, S. Doniach, and J.A. Spudich. 2008. Dynamic charge interactions create surprising rigidity in the ER/K alpha-helical protein motif. *Proc Natl Acad Sci U S A*. 105:13356-13361.

Solc, C.K., B.H. Derfler, G.M. Duyk, and D.P. Corey. 1994. Molecular cloning of myosins from the bullfrog saccular macula: a candidate for the hair cell adaptation motor. *Auditory Neuroscience*. 1:63-75.

Sousa, A.D., J.S. Berg, B.W. Robertson, R.B. Meeker, and R.E. Cheney. 2006. Myo10 in brain: developmental regulation, identification of a headless isoform and dynamics in neurons. *J Cell Sci*. 119:184-194.

Sousa, A.D., and R.E. Cheney. 2005. Myosin-X: a molecular motor at the cell's fingertips. *Trends Cell Biol*. 15:533-539.

Sun, Y., O. Sato, F. Ruhnow, M.E. Arsenault, M. Ikebe, and Y.E. Goldman. 2010. Single-molecule stepping and structural dynamics of myosin X. *Nat Struct Mol Biol*. 17:485-491.

Svitkina, T.M., E.A. Bulanova, O.Y. Chaga, D.M. Vignjevic, S. Kojima, J.M. Vasiliev, and G.G. Borisy. 2003. Mechanism of filopodia initiation by reorganization of a dendritic network. *J Cell Biol*. 160:409-421.

Sydor, A.M., A.L. Su, F.S. Wang, A. Xu, and D.G. Jay. 1996. Talin and vinculin play distinct roles in filopodial motility in the neuronal growth cone. *The Journal of cell biology*. 134:1197-1207.

Tacon, D., P.J. Knight, and M. Peckham. 2004. Imaging myosin 10 in cells. *Biochem Soc Trans*. 32:689-693.

Tilney, L.G., D.J. Derosier, and M.J. Mulroy. 1980. The organization of actin filaments in the stereocilia of cochlear hair cells. *J Cell Biol*. 86:244-259.

Tokuo, H., and M. Ikebe. 2004. Myosin X transports Mena/VASP to the tip of filopodia. *Biochem Biophys Res Commun*. 319:214-220.

Tokuo, H., K. Mabuchi, and M. Ikebe. 2007. The motor activity of myosin-X promotes actin fiber convergence at the cell periphery to initiate filopodia formation. *J Cell Biol*. 179:229-238.

Toyoshima, F., and E. Nishida. 2007. Integrin-mediated adhesion orients the spindle parallel to the substratum in an EB1- and myosin X-dependent manner. *Embo J*. 26:1487-1498.

Trybus, K.M. 2008. Myosin V from head to tail. *Cell Mol Life Sci*. 65:1378-1389.

Tyska, M.J., and M.S. Mooseker. 2002. MYO1A (Brush Border Myosin I) Dynamics in the Brush Border of LLC-PK1-CL4 Cells. *Biophys J*. 82:1869-1883.

Vitriol, E.A., A.C. Uetrecht, F. Shen, K. Jacobson, and J.E. Bear. 2007. Enhanced EGFP-chromophore-assisted laser inactivation using deficient cells rescued with functional EGFP-fusion proteins. *Proceedings of the National Academy of Sciences of the United States of America*. 104:6702-6707.

Walsh, T., V. Walsh, S. Vreugde, R. Hertzano, H. Shahin, S. Haika, M.K. Lee, M. Kanaan, M.C. King, and K.B. Avraham. 2002. From flies' eyes to our ears: mutations in a human class III myosin cause progressive nonsyndromic hearing loss DFNB30. *Proc Natl Acad Sci U S A*. 99:7518-7523.

Wang, F.S., J.S. Wolenski, R.E. Cheney, M.S. Mooseker, and D.G. Jay. 1996. Function of myosin-V in filopodial extension of neuronal growth cones. *Science*. 273:660-663.

Wang, J.J., X.Q. Fu, Y.G. Guo, L. Yuan, Q.Q. Gao, H.L. Yu, H.L. Shi, X.Z. Wang, W.C. Xiong, and X.J. Zhu. 2009. Involvement of headless myosin X in the motility of immortalized gonadotropin-releasing hormone neuronal cells. *Cell Biol Int*. 33:578-585.

Watanabe, T.M., H. Tokuo, K. Gonda, H. Higuchi, and M. Ikebe. 2010. Myosin-X induces filopodia by multiple elongation mechanism. *J Biol Chem*. 285:19605-19614.

Weber, K.L., A.M. Sokac, J.S. Berg, R.E. Cheney, and W.M. Bement. 2004. A microtubule-binding myosin required for nuclear anchoring and spindle assembly. *Nature*. 431:325-329.

Wei, Z., J. Yan, Q. Lu, L. Pan, and M. Zhang. 2011. Cargo recognition mechanism of myosin X revealed by the structure of its tail MyTH4-FERM tandem in complex with the DCC P3 domain. *Proc Natl Acad Sci U S A*.

Wood, W., and P. Martin. 2002. Structures in focus--filopodia. *Int J Biochem Cell Biol*. 34:726-730.

Woolner, S., L.L. O'Brien, C. Wiese, and W.M. Bement. 2008. Myosin-10 and actin filaments are essential for mitotic spindle function. *J Cell Biol*. 182:77-88.

Wu, L., L. Pan, Z. Wei, and M. Zhang. 2011. Structure of MyTH4-FERM domains in myosin VIIa tail bound to cargo. *Science*. 331:757-760.

Wu, X., F. Wang, K. Rao, J.R. Sellers, and J.A. Hammer, 3rd. 2002. Rab27a is an essential component of melanosome receptor for myosin Va. *Mol Biol Cell*. 13:1735-1749.

Wuhr, M., T.J. Mitchison, and C.M. Field. 2008. Mitosis: new roles for myosin-X and actin at the spindle. *Curr Biol*. 18:R912-914.

Yang, Y., T.G. Baboolal, V. Siththanandan, M. Chen, M.L. Walker, P.J. Knight, M. Peckham, and J.R. Sellers. 2009. A FERM domain autoregulates Drosophila myosin 7a activity. *Proc Natl Acad Sci U S A*. 106:4189-4194.

Yonezawa, S., A. Kimura, S. Koshiba, S. Masaki, T. Ono, A. Hanai, S. Sonta, T. Kageyama, T. Takahashi, and A. Moriyama. 2000. Mouse myosin X: molecular architecture and tissue expression as revealed by northern blot and in situ hybridization analyses. *Biochem Biophys Res Commun*. 271:526-533.

Yonezawa, S., N. Yoshizaki, M. Sano, A. Hanai, S. Masaki, T. Takizawa, T. Kageyama, and A. Moriyama. 2003. Possible involvement of myosin-X in intercellular adhesion: importance of serial pleckstrin homology regions for intracellular localization. *Dev Growth Differ*. 45:175-185.

Yu, C., W. Feng, Z. Wei, Y. Miyanoiri, W. Wen, Y. Zhao, and M. Zhang. 2009. Myosin VI undergoes cargo-mediated dimerization. *Cell*. 138:537-548.

Zamir, E., and B. Geiger. 2001. Molecular complexity and dynamics of cell-matrix adhesions. *Journal of cell science*. 114:3583-3590.

Zhang, H., J.S. Berg, Z. Li, Y. Wang, P. Lang, A.D. Sousa, A. Bhaskar, R.E. Cheney, and S. Stromblad. 2004. Myosin-X provides a motor-based link between integrins and the cytoskeleton. *Nat Cell Biol*. 6:523-531.

Zheng, L., G. Sekerkova, K. Vranich, L.G. Tilney, E. Mugnaini, and J.R. Bartles. 2000. The deaf jerker mouse has a mutation in the gene encoding the espin actin-bundling proteins of hair cell stereocilia and lacks espins. *Cell*. 102:377-385.

Zhu, X.J., C.Z. Wang, P.G. Dai, Y. Xie, N.N. Song, Y. Liu, Q.S. Du, L. Mei, Y.Q. Ding, and W.C. Xiong. 2007. Myosin X regulates netrin receptors and functions in axonal path-finding. *Nat Cell Biol*. 9:184-192.

Zhuravlev, P.I., B.S. Der, and G.A. Papoian. 2010. Design of active transport must be highly intricate: a possible role of myosin and Ena/VASP for G-actin transport in filopodia. *Biophysical journal*. 98:1439-1448.